preprint version of: Annu. Rep. NMR Spectrosc. 92, 137-198 (2017), published version © 2017 Elsevier Ltd.
link to published version: https://doi.org/10.1016/bs.arnmr.2017.04.002

Recent NMR Studies of Thermoelectric Materials

Ali A. Sirusi[a]*, Joseph H. Ross Jr.[a,b†]

[a]*Department of Physics and Astronomy, Texas A&M University, College Station, Texas 77843, USA*
[b]*Department of Materials Science and Engineering, Texas A&M University, College Station, Texas Texas 77843, USA*

Abstract

Thermoelectric materials can directly convert heat to electricity and are expected to lead to new devices to harvest waste heat for energy efficiency, as well as new cooling technologies. Optimization of these properties requires tailoring vibrational properties as well as the entropy carried by electrical charges and spins. NMR measurements have been important for understanding these processes, providing a measure of anharmonic "rattling" phonon behavior, local fluctuations in charge carrier and magnetic properties, and atomic-scale symmetries and distortions within these materials. Here we report recent NMR results focusing on inorganic clathrates, skutterudites, oxides, noble metal chalcogenides, complex tellurides, and half-Heusler compounds in which high thermoelectric efficiencies have been reported.

Contents

1 Introduction 2
1.1 Thermoelectric Materials Overview 2
1.2 NMR Concepts and Applications in Thermoelectric Systems 3
1.2.1 NMR Line Shapes and Computational tools. 4
1.2.2 Charge Carriers, Knight Shifts, and Korringa Response 6
1.2.3 Pseudogap and Resonant Behaviour 9
1.2.4 Quadrupole Relaxation; Rattling 10
1.2.4 Superionic motion 12
2 Specific Materials Systems 14
2.1 Inorganic clathrate compounds: 14
2.2 Skutterudite compounds 20
2.3 Noble Metal Chalcogenides 24
2.4 Oxide compounds 26
2.5 Bi, Pb, and Ge Tellurides. 30
2.6 Half-Heusler Compounds 32
Conclusions 34
Acknowledgements 35
References 35

* Now at Department of Biochemistry and Molecular Biology, University of Florida, *E-mail address*: alisirusi@ufl.edu.
† Corresponding author. fax: +1-979-845-2590, *E-mail address*: jhross@tamu.edu.

1 Introduction

1.1 Thermoelectric Materials Overview

Thermoelectric materials can harvest waste heat and directly convert it to electricity. In addition, the reverse process corresponding to the Peltier effect can lead to efficient solid-state cooling, potentially replacing chlorofluorocarbon-based refrigerants or allowing active cooling of microdevices. Furthermore it is believed that there are ways to optimize this behavior for significant enhancement of these properties, and thus there has been great interest in recent years in improved materials for these applications. A brief overview is given here of the materials and terminology; readers are referred to several excellent recent reviews [1–6] for more information.

Thermoelectricity is a well-known concept since the work of Seebeck [7,8] and Peltier [9] in the 1820s. Seebeck showed that by applying a temperature gradient across a conductor, one can generate a voltage. This is the basis for the thermocouple sensor. The ratio of the generated voltage to the temperature gradient is called Seebeck coefficient (*S*). The sign of the Seebeck coefficient usually reflects the carrier type, for example an n-type semiconductor has a negative value. Despite knowledge of the effect for many years, the first application was recognized in the 1950s after discovery of high efficiency thermoelectric behavior in bismuth tellurides [4,5]. The parameter that determines the efficiency of thermoelectric processes is called the figure of merit (zT), which can be expressed as

$$zT = \sigma S^2 T / k \qquad (1)$$

where the σ is the electrical conductivity, and k is the thermal conductivity. The thermal conductivity can be writtern as $k = k_{latt} + k_{carrier}$, in which k_{latt} is the lattice thermal conductivity related to lattice vibrations, and $k_{carrier}$ is the electronic thermal conductivity due to the carriers. At high temperature, bipolar terms also can be added to the electronic thermal conductivity.

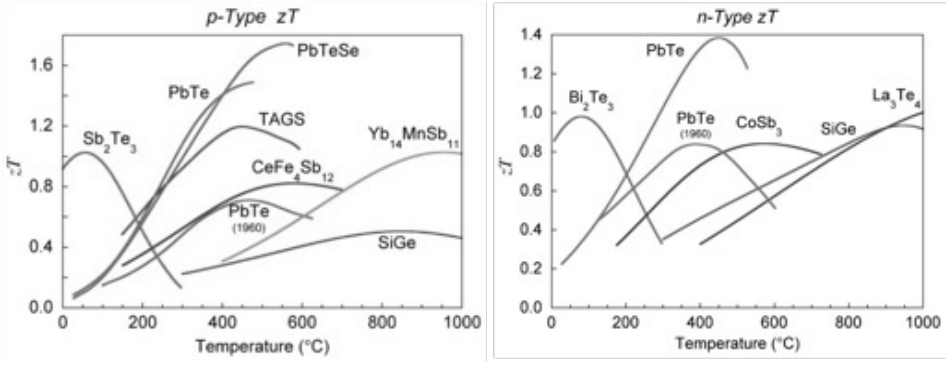

Figure 1: Comparison of *n*- and *p*-type figure of merits of selected thermoelectric materials. Adapted by permission from Macmillan Publishers Ltd: Nature Materials [10], © 2008.

Materials can be considered as promising thermoelectrics if they have zT as large as possible, with $zT = 1$ typically a minimum targeted value for practical consideration. From (1) is seen that achieving high zT requires high power factor (σS^2) and low thermal conductivity.

There are many challenges to optimizing the power factor and minimizing k independently. S and σ have different relations with the carrier density and as a result the power factor typically has a maximum in the range 10^{18}-10^{20} cm^{-3}. Also large σ generally implies large $k_{carrier}$, so minimizing the denominator of (1) normally means tailoring the phonon contributions to k_{latt}. Figure 1 displays the figures of merit of some of the promising thermoelectric materials vs temperature. Recently there have been many strategies explored to increase the zT [1]. These include band convergence (for example, PbTe at high temperature [11]), and electron resonant states (Al-doped PbSe [12]). Magnetic spin entropy can also contribute to an enhanced power factor (as in the cobalt oxides discussed below [13]), or as recently proposed Rashba spin-orbit effects (BiTeI [14]). Phonon transport may be tailored through rattling in caged compounds (clathrates [15]), as well as other types of strong anharmonicity in the crystal (SnSe [16]), and there are other means of reduction of the thermal conductivity by introduction of microstructures and/or engineered nanostructures, or liquid-like ions [17].

Since optimizing these conditions often leads to complex, nonstoichiometric and/or mixed-phase materials, a local probe such as NMR can be invaluable for understanding the local atomic environment and symmetries underlying the macroscopic thermoelectric properties. In addition, NMR provides a site-selective measure of the charge-carrier behaviour, as well as of phonons and thermally-induced atomic dynamics within these systems. In this report, we will review the NMR data of new thermoelectric materials, with a focus specifically on inorganics. These include inorganic clathrates, skutterudites, oxides, and half-Huesler compounds, as well as superionic conductors and complex telluride materials. A large list of thermoelectric materials can be found in Ref. [18] as well as in the general reviews cited above.

1.2 NMR Concepts and Applications in Thermoelectric Systems

The interactions determining the NMR spectrum are classified by the following terms in the Hamiltonian:

$$H_{\text{total}} = H_{\text{Z,ext}} + H_{\text{contact}} + H_{\text{orbital}} + H_{\text{spin-dipolar}} + H_{\text{nuclear-nuclear}} + H_{\text{quadrupole}}, \quad (2)$$

where the electric quadrupole term ($H_{\text{quadrupole}}$) is only present for nuclei with spin 1 or greater, and all other terms have their origins in magnetic interactions of the nuclei with the electrons or applied field. Note that in absence of an applied field (the first term), some quadrupole systems may be studied through nuclear quadrupole resonance (NQR), rather than NMR; a few such results are also included in this review. The second and third term in (2) make the largest magnetic contribution to the NMR shifts; shifts due to the Fermi contact term (H_{contact}) will be identified here as Knight shifts (K), normally due to conduction electrons and holes, although in magnetic materials the local magnetization also contributes to this term. Defining the chemical shift (δ) to be the contributions due the H_{orbital} term, the total magnetic shift is given by $K + \delta$, and assuming sufficiently weak spin-orbit coupling that the orbital susceptibility is independent of the spin susceptibility.

1.2.1 NMR Line Shapes and Computational tools.

There has been considerable development of methods to calculate NMR lineshape parameters through density functional techniques (DFT), or other quantum chemical techniques. Currently a number of available DFT packages include capabilities allowing users to compute both the electric field gradients (EFGs) determining quadrupole shifts, and also the chemical shifts. These are becoming increasingly important for assigning spectral features to different sites or phases in thermoelectric alloys and complex thermoelectric materials. For computation of the EFG's using such packages as WIEN2k [19] there is by now an extensive literature to which to compare the results, and it is possible to obtain reliabile results by following established procedures. As example, Figure shows a wide-line quadrupole ^{27}Al NMR spectrum [20] for a sample of $Ba_8Al_{12}Ge_{33}$, a cage-type inorganic clathrate of the class of materials discussed in section 2.1 below. Modeling the mixed occupancy of Al, Ge, and vacancies on three framework sites as superstructures with a number of overlapping sites, the best fitting spectra in this case were also found in good agreement with most stable configurations computed by DFT methods. Similar methods were used for $Ba_8Ga_xSn_{46-x}$ clathrates [21]. This allows such local features as correlations between neighboring site occupation to be addressed. The results in this case showed that the splitting of the central (1/2,–1/2) transition could be attributed to Al-vacancy combinations, and indicated the importance of Al nonbonding states near the Fermi edge in this system [20].

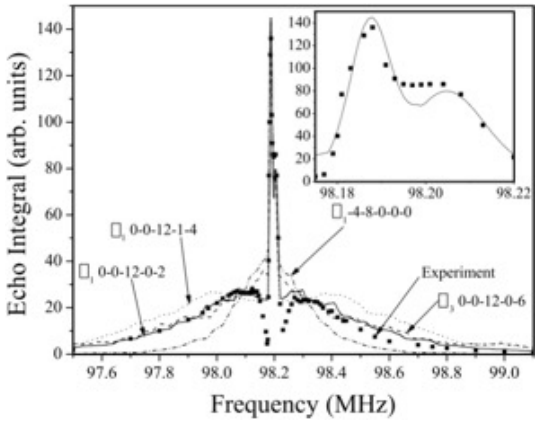

Figure 2: Wide-line ^{27}Al powder NMR spectrum for the type-I clathrate $Ba_8Al_{12}Ge_{33}$, with central transition shown in expanded view in inset, along with several computed mixed-occupancy spectra, calculated in WIEN2k code. Curves are labelled for site occupancy and nearest-neighbour configurations as defined in [20]. Reprinted with permission from [20], © 2009 American Physical Society.

Similar computational tools were used for example by Gippius et al. [22], addressing local distortions at filler sites in skutterudites. Skutterudites are discussed in more detail in section 2.2, and the configuration of the filler atoms is believed to play a large role in phonon propagation and the possible anharmonic rattling behavior of importance for the thermal conductivity. In measurements of ^{139}La and ^{23}Na NMR and ^{121,123}Sb-NQR as a function of temperature on

MFe_4Sb_{12} (M = La, Ca, and Na) samples, as Figure 3 shows, a splitting into two peaks develops at low temperatures. This occurs most prominently for the La-filled material, and the result is attributed to spontanous displacemens of the filler atoms and thus symmetry reduction. Calculations of the EFG's for the Sb NQR peaks were used to confirm this analysis. Similar to the case for the clathrate system, the presence of random disorder in filler site positioning has significant implications for the carrier mobility as well as for the vibrational behaviour, and thus the ability to probe and model this behavior is quite important in optimizing *zT* in these systems.

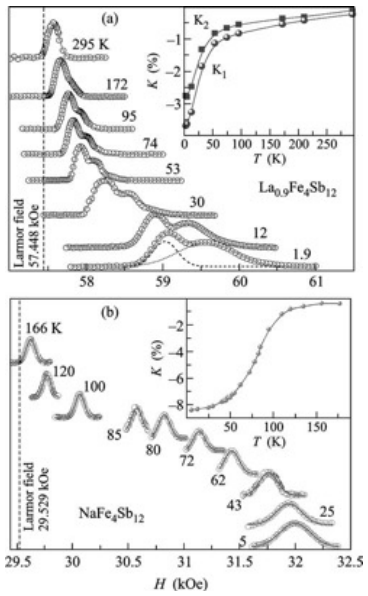

Figure 3: (a) ^{139}La spectrum of $LaFe_4Sb_{12}$ (b) ^{23}Na spectrum of $NaFe_4Sb_{12}$; splitting/broadening of spectrum is attributed to low-temperature distortion of structure due to off-centering of cage-filler atoms. Reprinted with permission from [22], © 2009 Pleiades Publishing, Ltd.

For modeling of the chemical shifts in crystalline systems, such techniques as GIPAW [23] wave functions can be used. As opposed to the treatment of molecular systems for which gauge invariance is not an issue, the capabilities for such calculations have come online relatively recently in DFT-based computational packages for extended systems. For example Baran et al. [24] recently used GIPAW methods in order to confirm the site assignments for ^{27}Al MAS-NMR spectra measured for several $A_8Al_8Si_{38}$ compositions. These are clathrate materials with the same general type-I structure as $Ba_8Al_{12}Ge_{33}$ (Figure), and in this case the average Al occupation of the 3 categories of framework sites can be seen directly through the appearance of three separated lines in the ^{27}Al NMR spectrum, with results seen in Figure . In this work use of GIPAW computational tools allowed confirmation of the assignment of these lines to the individual sites. As an alternative method, for PbTe semiconductors the ADF package was used to calculate large clusters approximating the local environment within the crystal, following a relativistic calculation with spin-orbit coupling included [25]. The ability to include spin-orbit effects is increasingly important for heavy-element semiconductors such as PbTe, beacause of the realization of the presence of topological insulator behaviour in this and related materials, and for this reason understanding the NMR shifts in such materials is currently an area of significant interest. Furthermore, thermoelectrics as a class often contain heavy atoms for which relativistic effects

may be significant. However, caution may be needed in interpreting new results since spin-orbit effects are currently not fully implemented in some of the available computation packages.

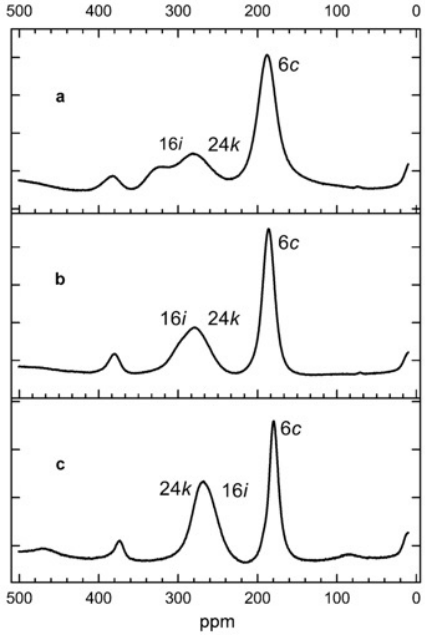

Figure 4: ^{27}Al MAS-NMR spectra for several $A_8Al_8Si_{38}$ clathrate samples. Labels show site assignments for Al occupation of 3 main framework sites within the type-I clathrate structure. Reprinted with permission from [24], © 2014 Wiley-VCH Verlag GmbH & Co. KGaA, Weinheim.

1.2.2 Charge Carriers, Knight Shifts, and Korringa Response

As noted above, efficiency requirements for thermoelectric materials lead to targeted ranges of carrier densities. Normally this leads to materials which are considered semiconductors, although at the optimized range of carrier densities these are often heavily-doped and thus actually behave as dilute metals, exhibiting for example a positive temperature coefficient of resistivity. The Knight shifts can thus be very significant, with K a large part of the observed shifts. In this limit T is considerably smaller than the Fermi temperature, $T_f = \hbar^2(3\pi^2 n)^{2/3}/[2m^* k_B]$, where n the carrier density and m^* the effective mass. Korringa behavior is thus expected, characterized by a temperature-independent K, and a corresponding contribution T_1T = constant [26,27]. In more dilute or higher temperature cases, classical statistics may hold giving $1/T_1 \propto n\sqrt{T}$, and with $n \propto T^{3/2}e^{-E_g/k_BT}$, this leads to $1/T_1 \propto T^2 e^{-E_g/k_BT}$ as long as the conductor is in the intrinsic regime. However, note that in this regime carrier localization or in some cases impurity bands can be important, leading to a variety of rather different behaviors reported for NMR in semiconductors below the metal-insulator limit, such as described in references [28–30].

An example of metallic behavior is shown in Figure for the half-Heusler material CoTiSb [31]. While electron-counting rules for the half Heuslers suggest that this material may be a semiconductor or semimetal, the T_1T = constant behavior, consistent with the observed low-temperature shifts, show that there is a nonzero metallic density of states at the Fermi level ($g(E_f)$). These results demonstrated that the residual $g(E_f)$ is strongly dependent on sample processing, and further help to show that observed changes in transport behavior are associated with the annealing away of active defects rather than composition changes. The increase in both K and 1/ T_1T above

the low-temperature metallic region is attributed to pseudogap behavior, discussed in more detail below, with an enhancement in carriers vs. increasing temperature due to E_f occurring within a narrow gap.

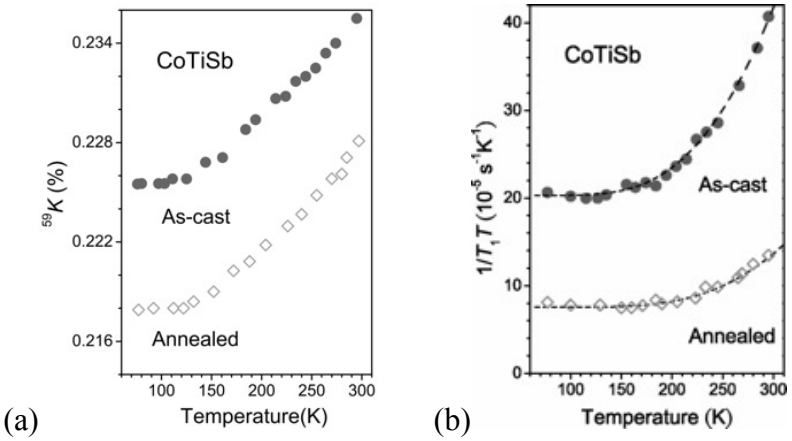

Figure 5: ^{59}Co NMR results for half-Heusler CoTiSb, measured for as-cast and annealed samples as shown. (a) shifts vs. T; (b) $1/T_1T$ product. Reprinted with permission from [31], © 2009 American Physical Society.

In the Korringa limit the Knight shift can be given very generally as

$$K = \mu_B g_{\text{partial}}(E_f)(g^*/g_o)B_{HF}, \qquad (3)$$

where μ_B is the Bohr magneton, B_{HF} is the relevant hyperfine coupling constant, for example involving Fermi contact for s-symmetry orbitals for the case of normal metals, and $g_{\text{partial}}(E_f)$ is the Fermi-level partial density of states for the atom containing the nucleus being measured. For the case of s-contact interactions determining K in simple metals, this would be $g_s(E_f)$, representing the local s-symmetry contribution. Also in (3) the effective g-factor g^* is due to spin-orbit coupling, which modifies the energy splitting and thus the spin susceptibility [32] correspondingly also modifies K. This term can be particularly important for narrow-gap and small mass systems, for which g^* can differ significantly from $g_o = 2$, for example as found in the unfilled skutterudite $CoSb_3$ [33].

Determination of the product contained in Eqn. (3) has in recent years become possible with reasonable expected accuracy through computational means by using available density functional theory packages [34] although the spin-orbit contribution remains difficult to obtain in this way. More commonly, and for complex materials for which direct computation is not possible, this relation can be used to obtain an approximate estimate of $g_{\text{partial}}(E_f)$ using fields B_{HF} obtained for specific elements [26,35]. Experimentally the Knight shift contribution can be identified by measuring a series of samples with known carrier densities and extrapolating to zero to obtain δ. In an effective mass approximation, which is often appropriate for semiconductors, it is found in the metallic limit, $g(Ef) = m^*(3\pi^2 n)^{1/3}/(\hbar^2\pi^2)$, where m^* is the thermodynamic effective mass and n the carrier density. Thus using eqn. (3) K should scale as $n^{1/3}$. This scaling has been demonstrated in isolated cases for specific semiconductors [36] and see also the recent review [37] of NMR in semiconductors for additional information.

An interesting method was used by Sakurai *et al*. [38] to determine the ^{121}Sb Knight shifts in Sr and Ca filled $FeSb_3$, In this case due to the very large quadrupole shifts for the Sb nucleus, K was measured by applying a series of small fields and analyzing the resulting splitting in the NQR line, as shown in Figure 6(a). Results are shown in part (b) of the figure. Note that these correspond also to the filled skutterudite materials shown in Figure 3, but with different filler atoms. The large negative Knight shifts signify Fe spin fluctuations rather than metallic behaviour, and here signify strong covalent coupling between Sb and Fe orbitals. However, although nominally ferromagnetic, these results show that there is a suppression of spin fluctuations at low temperatures, a result which is consistent with and explains previous T_1 measurements. These materials are important for potential themoelectric appications, and the spin-hybridization properties also lead to heavy quasiparticle behavior in these and related Fe-based skutterudites, nearly as large as observed in rare-earth-based Heavy fermion materials [39].

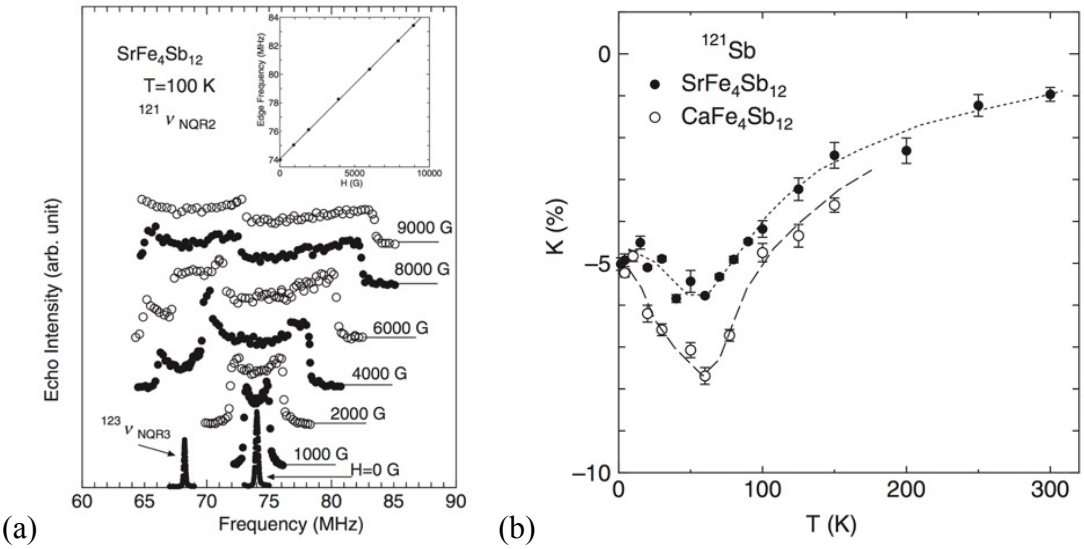

Figure 6: ^{121}Sb Knight shifts for filled $FeSb_3$ skutterudites. (a) line shapes showing field-induced splitting of NQR signals. (b) Results for K vs. temperature. Reprinted with permission from [38], © 2008 The Physical Society of Japan.

For the case of metallic behavior, the Korringa product is,

$$K^2 T_{1M} T = S_K \hbar \gamma_e^2 / (4\pi k_B \gamma_n^2), \qquad (4)$$

where γ_n and γ_e are the nuclear and electronic gyromagnetic ratios. In this case, T_{1M} is specifically the metallic contribution to T_1 in cases where multiple terms contribute to the relaxation, and S_K is an enhancement factor related to electron-electron interactions [26,35]. S_K is often not known, and it may differ considerably from 1 in the case of dilute carrier-density semiconductors [40], or in materials where strong interaction effects or spin fluctiuation behavior may be expected, such as observed in $NdOs_4P_{12}$ skutterudite [41]. In the case that an effective mass treatment is appropriate for materials in the Korringa regime, from an analysis similar to what is given above for K one finds that $(1/T_{1M})$ should scale as $n^{2/3}$ for samples with different carrier densities, and typically when the Korringa contribution can be identified, there is less ambiguity since there is no added chemical shift conribution to T_1. This scaling has been used, for example in Cu_2Te to analyse the

electronic behavior [42], as shown in Figure . In this case p is the hole density and T_{1M} is measured in the centre portion of the line (Figure). It was established [43] for this material that Korringa behavior dominates at low temperatures, whereas approaching room temperture a quadrupole mechanism takes hold due to slow hopping of the Cu ions, which also leads to the decreased spin-echo signal shown in Figure (a). T_1 measurements in a series of TAGS samples were also used [44] as a means to analyse for variations in effective mass m^* as well as n, in that case with classical statistics rather than Fermi for the carriers. TAGS represents the series of Ag and Sb substituted GeTe themoelectrics discussed in section 2.5, known for high zT response (Figure 2).

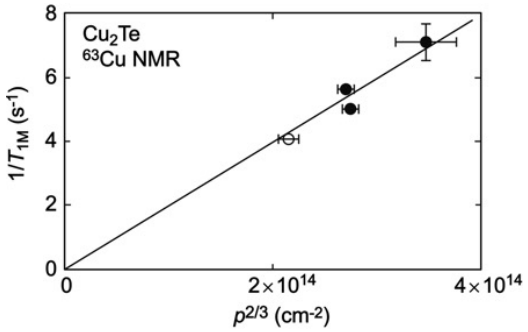

Figure 7: ^{63}Cu magnetic spin-lattice relaxation rate for $Cu_{2-x}Te$ materials. Plotted vs. $p^{2/3}$, the linearity corresponds to effective mass behaviour of hole pockets due to carriers donated by Cu vacancies with increasing x. Reprinted with permission from [42], © 2017 Elsevier Ltd.

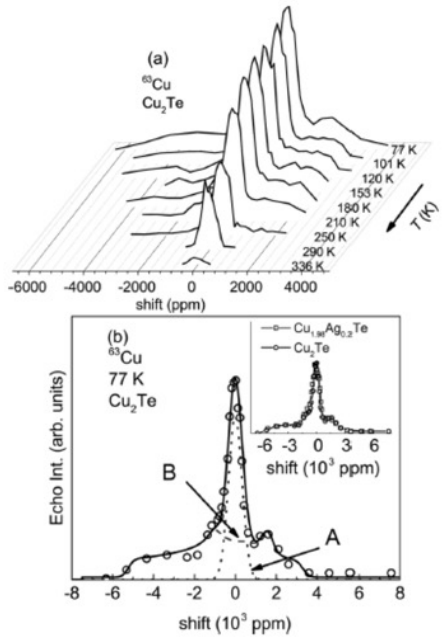

Figure 8: ^{63}Cu NMR spectra for $Cu_{2-x}Te$ [43]: (a) temperature dependence, with hopping-induced decrease in echo signal seen approaching room temperature; (b) 77 K spectrum, with fitting to two Cu sites. Reprinted with permission from [43], © 2016 American Chemical Society.

1.2.3 Pseudogap and Resonant Behaviour

A pseudogap in the electronic density of states was discussed previosly as identified with the upturn in relaxation rate and Knight shift seen in Figure [31], and such changes at low temperatures often signify narrow and/or sharply defined features in $g(E)$ near E_f. Such features can strongly enhance the thermoelectric zT , for example simple transport models indicate that large curvature of $g(E)$ can strongly enhance S. For similar reasons resonant states in $g(E)$ are expected to enhance the thermoelectric efficiency [45]. Resonant features may include resonances such as related to the Kondo effect, or hybridization processes such as occur in more dense Kondo systems such as the heavy-Fermion skutterudite $YbFe_4Sb_{12}$ [46]. Alternatively more traditional hybridization mechanism involving a relatively weakly connected atom may be responsible. NMR studies are an excellent way to probe such features [47].

By expanding $g(E)$ in derivatives of E, in the limit of a parabolic minimum [48,49] one finds NMR contributions given by $1/T_{1M} = aT + bT^3$, and also a T^2 additive contribution to K. Alternatively, treating $g(E)$ as corresponding to a semiconducting gap with a residual E-independent contribution to $g(E)$ inside the gap leads to $1/T_{1M} = cT + dT^2 e^{-E_g/k_B T}$. This is simply a sum of Korringa and classical-statistics terms; classical statistics would be expected to be valid in the limit of thermally-excited carriers. A similar sum is also obtained for K. Note also that this is distinct from the pseudogap behavior familiarly identified in high-T_c cuprates [50].

A parabolic pseudogap was recely identified in NMR studies of the high-zT clathrate $Ba_8Ga_{16}Ge_{30}$ by such methods using ^{69,71}Ga NMR [48], based both on changes in K and T_1. The pseudogap feature in this case is likely identified with weakly hybridized filler atom resonances falling within the conduction band. In the fully filled skutterudite $YbFe_4Sb_{12}$ on the other hand, Magishi et al. [51] detected presence a pseudogap through Sb NQR, based on the T_1 behavior superimposed on a magnetic contribution which could be matched to the measured susceptibility. In this case the pseudogap is identified with band crossing due to presence of the filler atom. Similarly, through ^{195}Pt T_1 measurements, it was identified [52] that the nominally semiconducting half-Heusler TiPtSn actually exhibits a pseudogap with residual density of carriers at the Fermi level. Furthermore recently in the high-efficiency thermoelectric TAGS-85 [53], ^{125}Te NMR results were highlighted as a possible indication of the presence of resonant levels in the conducton band.

1.2.4 Quadrupole Relaxation; Rattling

Aside from T_{1M}, other significant contributions to the T_1 come from electric quadrupole effects, for nuclei having $I \geq 1$. In thermoelectrics the mechanism for this contribution is typically the lattice vibrations, which play a very significant role in the thermoelectric efficiency as outlined above. Two parameters determine the relaxation rate in this case, one of which (W_1) relates to nuclear transitions with $\Delta m_z = \pm 1$, and the other (W_2) to $\Delta m_z = \pm 2$, however when fitted to an overall exponential recovery curve the rate may also be identified as $1/T_{1Q}$. Several techniques have been proposed to identify these terms and 1/ T_{1M} experimentally [54], but in general the rates scale according to W_1 and $W_2 \propto Q^2$, and $1/T_{1M} \propto \gamma_n^2$, where Q is the nuclear quadrupole moment. Thus for nuclear systems with two stable quadrupolar nuclei such as ^{63,65}Cu and ^{69,71}Ga, if one process dominates the mechanism determining the relaxation rate can be identified by measurements of both resonances. These techniques have been used to demonstrate the strongly

anharmonic "rattling" phonon behavior in $LaOs_4Sb_{12}$ [55] and in $Ba_8Ga_{16}Sn_{30}$ [56,57] as shown below.

Considering a caged filler atom as a loosely-held local oscillator, Dahm and Ueda [58] devised a model for the NMR T_1 in which the cage was considered to produce a quartic confining potential of the form $ax^2/2 + bx^4/4$, where the parameter a may have either sign. In an effective phonon approximation, this gives an effective temperature dependent local oscillator frequency, and a resulting model for $1/T_1$ which can exhibit a low-temperature peak, based on a dimensionless anharmonicity parameter β. This was used to model results for KOs_2O_6 [59], and for the skutterudite $LaOs_4Sb_{12}$ a subtraction of a magnetic contribution to T_1 deduced from the Sb NQR line the result (Figure) shows the characteristic T-independent $1/T_1T$ at high temperatures, however, no low-T peak in this case. Note that the high-temperature $1/T_1T$ in presence of such oscillators exhibits temperature dependence that would normally be associated with metallic behavior, and which is a typical for phonon-driven relaxation. NMR signatures of rattling behavior were also shown in results for the $Pr(Os_{1-x}Ru_x)_4Sb_{12}$ skutterudite [60].

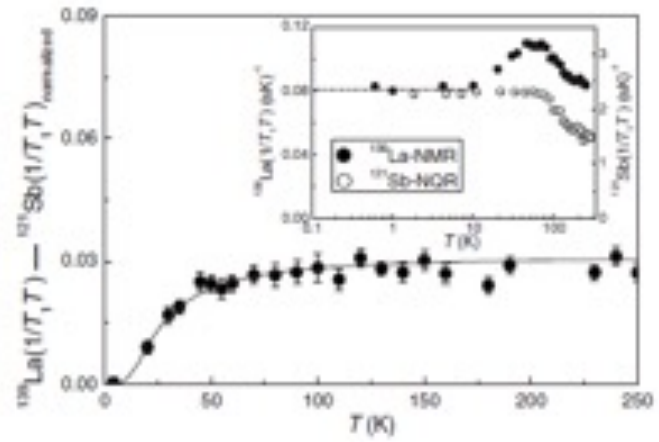

Figure 9: $(1/T_1T)$ difference for ^{139}La NMR vs ^{121}Sb NQR normalized rates [55] for $LaOs_4Sb_{12}$ skutterudite. Solid curve is fit to anharmonic local effective phonon "rattling" model [58]. Reprinted with permission from [55], © 2008 American Physical Society.

In the clathrate $Ba_8Ga_{16}Sn_{30}$, The Ga T_1^{-1} was shown to be dominated at low temperatures by quadrupole processes, and in this case to exhibit a large peak [56] as seen in Figure . This corresponds to a large anharmonicity in this system, which has particularly large cage sizes due to the expanded Sn-based framework, as well as very small thermal conductivity. This provides some validation for the model in which the filler atom is treated as an independent oscillator. Similar results were later obtained on several samples, including a single crystal [57] measurement.

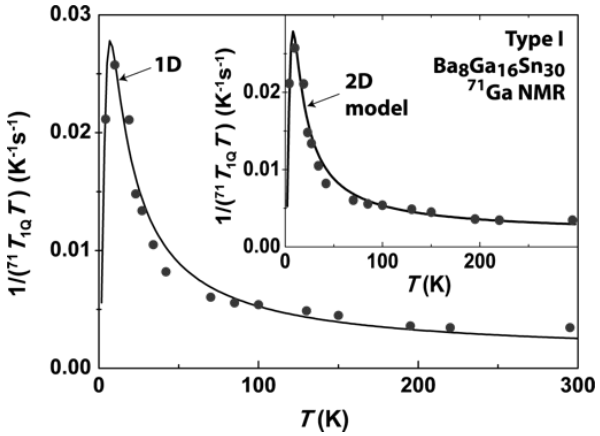

Figure 10: Ga quadrupole $1/(T_1T)$ for $Ba_8Ga_{16}Sn_{30}$, showing large "rattling" peak. Fits are to anharmonic effective-phonon model, with fits shown both for a 1 dimensional and a 2 dimensional anharmonic oscillator as indicated. Reprinted with permission from [56], © 2011 American Physical Society.

1.2.4 Superionic motion.

NMR is well-positioned to probe atomic motion within superionic and disordered materials [61,62], with typical NMR timescales allowing it to detect relatively long-timescale hopping, and also the ability to detect hopping in situ, and the development of phase segregation in these systems. In addition, in the last few years there has been a large growth in interest in Cu_2Se and related materials [17], as it was shown that the superionic/structural phase transition in Cu_2Se is concomitant with a large Seebeck coefficient enhancement. As discussed in section 2.3, this material is part of a family of chalcogenides which is of significant current interest for additional device-related and topological-based electronic behaviour. The thermoelectric response was modelled through a Cu-ion "liquid" acting as a basis for strong scattering of the phonons and thereby reducing the thermal conductivity significantly.

Cu_2Se has been long known as a superionic conductor, having a structural phase transition near 390 K. NMR was previously used [63,64] to measure the activation of Cu motion within the superionic regime, as shown in
Figure . The fitting is to an activated process, $1/T_1 \propto exp[-E_a/k_BT]$, providing a local measure of the hopping dynamics, and activation energies E_a comparable to results of macroscopic transport experiments. A wide-line, low temperature Cu NMR spectrum [65] is shown in Figure 4(a), with a comparison to the high-temperature spectrum which collapses to a single motionally-narrowed line, demonstrating the uniform liquid-like motion of the Cu ions in the crystal at high temperatures.

Figure 4(b) shows the change of ^{63}Cu spin-echo amplitude vs. temperature as hopping sets in. The amplitude reduction in the slow-motion regime is similar to the behavior shown in Figure for Cu_2Te. Fitting the echo dephasing results to an activated hopping process [65], however, did not yield results consistent with the measured high-temperature activation process, results related to a change in structure as also shown by the change in Knight shift (inset figure). On the other hand the Cu_2Te results [43] could be fitted to the same activated behaviour for the entire temperature

range from slow hopping to high temperature motional narrowing, indicating that a single activated process controls the dynamics in that case.

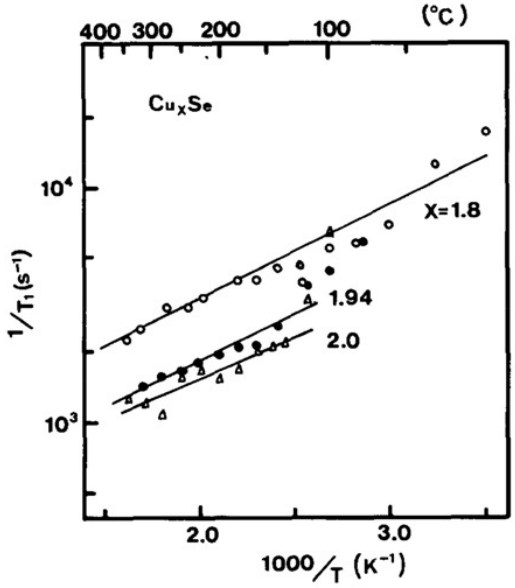

Figure 11: ^{63}Cu relaxation rates for Cu_xSe samples. Solid curves are fits to activated Cu-hopping behaviour in the superionic regime. Reprinted with permission from [64], © 1990 Elsevier Science Publishers B.V.

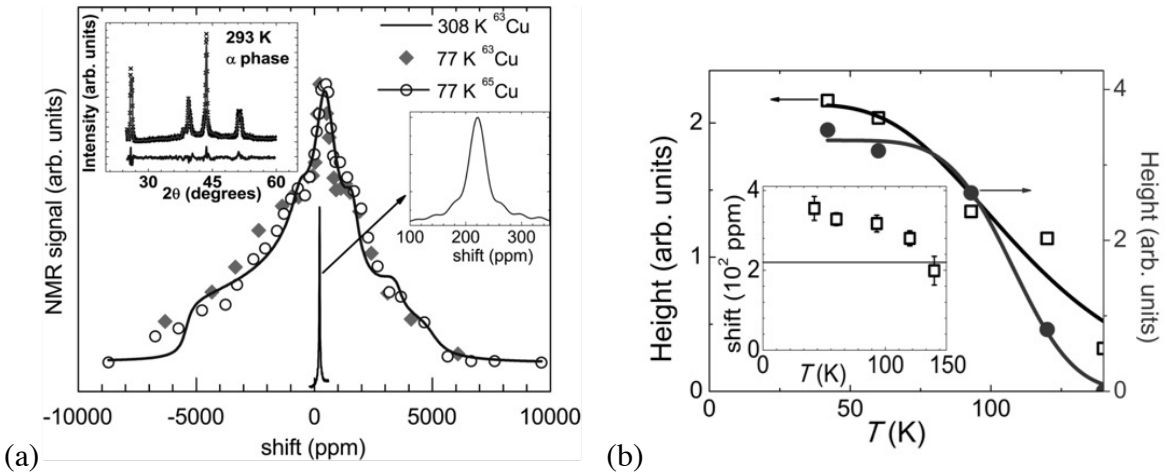

Figure 4: (a) ^{63}Cu spectra for Cu_2Se, showing superposition of static low- temperature spectra and motionally narrowed line near room temperature. (b) Change of spin echo height vs temperature for two fitted spectral components, demonstrating development of slow hopping, and (inset) change of Knight shift as Cu site symmetry changes in slow hopping regime. Reprinted with permission from [65], © 2015 American Chemical Society.

Aside from the noble metal chalcogenides discussed further in section 2.3, there is a wide range of Cu-based semiconductors which are currently of interest as thermoelectrics, of interest as basis for potentially earth-abundant as well as efficient devices. NMR has been quite useful in probing atomic dynamics, an issue which in many cases may degrade device performance. Among recent work, changes in Cu site symmetry near the superionic transformation was studied [66] by Cu

NMR in $Cu_2ZnGeSe_{4-x}S_x$, and in the high-zT half-Heusler MgAgSb [67] Mg NMR was used to indicate the presence of ion migration among Mg as well as Ag ions.

2 Specific Materials Systems

2.1 Inorganic clathrate compounds:

Intermetallic clathrates are cage-containing materials that can host guest atoms within the cages, with the guests in some cases serving as "rattler" ions. These compounds can have many different structures as shown in , and for the most part these are the same structures as the hydrate clathrates [15,68,69]. NMR studies addressing framework-site occupations, as well as anharmonic vibrational properties of $Ba_8Ga_{16}Sn_{30}$ clathrate, were already described above. A number of the clathrate compounds are recognized as potential thermoelectric materials, and interest in developing these materials has been due in part to the prospect of phonon-glass electron-crystal (PGEC) properties, with rattler atoms potentially inducing glass-like phonon scattering, but electrons responding more like those in crystals [70,71].

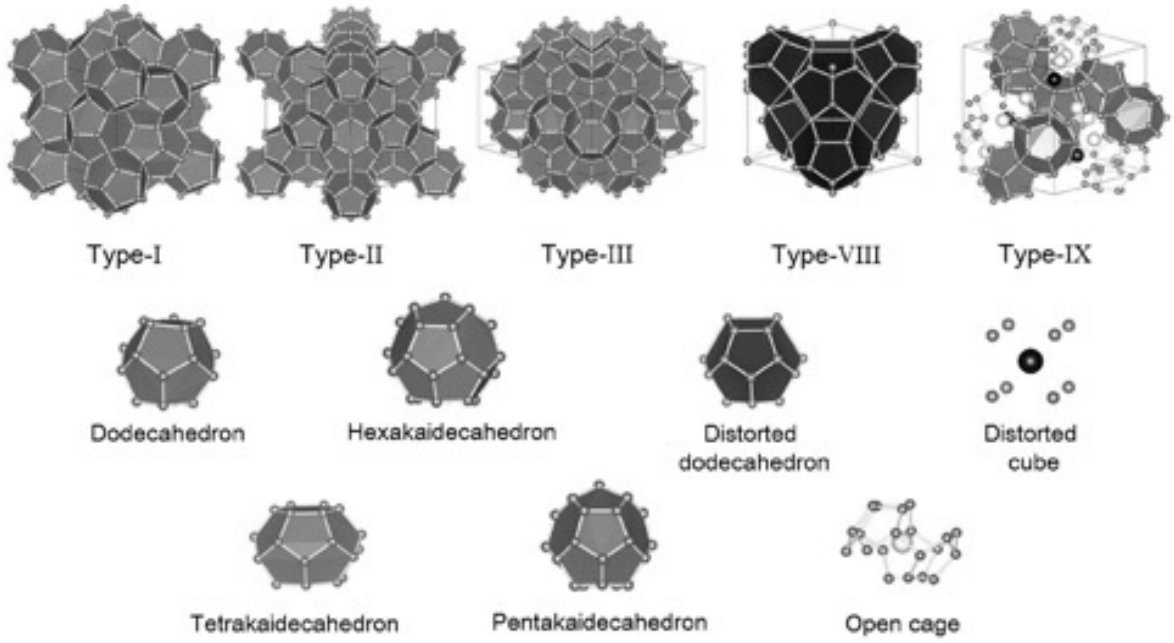

Figure 13: Clathrate structure types, along with some of the primitive cages making up these structures. Reprinted with permission from [15], © 2014 American Physical Society.

The type-I structure is the most common, with many different compositions exhibiting this structure. Type-I compounds with formula unit $R_8M_{16}Z_{30}$ have been extensively examined for thermoelectric applications, with for example an extrapolated zT has been quoted to be as large as 1.7 for $Ba_8Ga_{16}Ge_{30}$. In this case R atoms are from group-2, M from group-13, and Z from group-14, a configuration which gives electron balance and typically semiconducting behaviour. The framework atoms (M, Z) occupy 3 different sites (24k, 16i, and 6c; see Figure) and have nominally sp^3 covalent bonding. The guest atoms are encapsulated at 6d and 2a sites (Figure). The thermal

conductivity can depend greatly on the cage sizes, and in some cases the off-centre positioning of the guests, addressed for example by Suekuni *et al*. [72], showing that by increasing the Ge content in $Sr_8Ga_{16}Si_{30-x}Ge_x$, the thermal conductivity can change from crystal-like to glass-like characteristics. However, the off- and on-centre concept cannot explain the large difference in thermal conductivity of *p*-type $Ba_8Ga_{16}Ge_{30}$ vs. *n*-type $Ba_8Ga_{16}Ge_{30}$ [15], and recent results such as in reference [73] indicate strongly scattering phonon modes which may appear even in unfilled clathrates, so there may be multiple mechanisms associated with the low thermal conductivity in these systems.

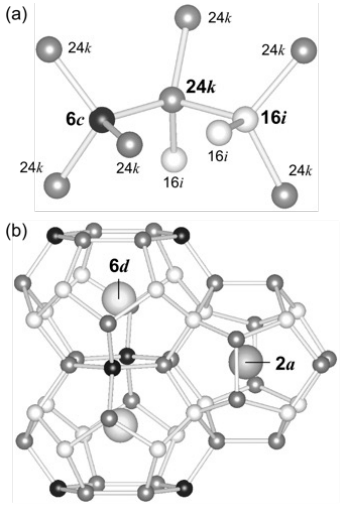

Figure 14: Site details for type-I clathrate structure. Reprinted with permission from [15], © 2014 American Physical Society.

Other relevant structures () include clathrates II ($A_{24}Z_{136}$), VIII (A_8Z_{46}), and IX ($A_{25}Z_{100}$). Type II includes semiconducting compositions with larger cages, but has been synthesized less commonly, in selected compositions. Type IX clathrates are generally metallic, and have been of particular interest for superconducting and magnetic properties rather than thermoelectric. In addition, type-I Ba_8Si_{46} and $Na_xBa_ySi_{46}$ are metallic and exhibit superconducting transitions with T_c as large as 8 K, a motivating subject for a number of NMR studies.

Silicon Clathrates: Clathrates can be classified according to the framework elements, including Si-based, Ge-based, Sn-based, and tetrel-free classifications. While Si clathrates traditionally pose more difficulties in establishing high-*zT* behavior since heavier elements and larger cages tend to produce lower thermal conductivities, the Si-based clathrates are desirable for potential TE applications since Si is a cheap and abundant element. A number of ^{29}Si NMR studies have been performed in Si clathrates, and shift results are summarized in Table 1. For type-I Si-based materials, the ^{29}Si NMR resonance shifts are from 600 ppm to 2200 ppm. These are much larger than in insulating silicides (0-130 ppm) [74], the difference indicating the metallic features of the type-I Si clathrates. Type-II Si clathrates can be produced with a wide range of filler-atom concentrations, and the resonance shift positions depend strongly on the guest atom concentration. For example, $Na_{24}Si_{136}$ has ^{29}Si resonance shifts in the range 600-850 ppm while in the nearly

unfilled material Na_xSi_{136} (x = 0.0058) the ^{29}Si NMR shift is up to 90 ppm, the difference presumably a Knight shift due to donated electrons from Na^+ ions filling conduction bands. However, surprisingly the ^{23}Na NMR positions for the filler atoms in Si clathrates correspond to very large Knight shifts (see Table 2), and these results provided strong evidence that the Na filler atoms in this case are not totally ionized as initially expected, but instead are hybridized with the conduction band with a large *s*-conduction electron density residing on the filler atom.

The first NMR data on the Si-based clathrates were obtained by Shimizu *et al*. [75] and Gryko *et al*. [76] on Si-based type-I and type-II clathrates with Na and Ba atoms as the guest atoms. A common feature was the result that the ^{29}Si and ^{23}Na nuclei have large Knight shifts due to a Fermi contact term, as noted above. The $Na_{2.9}Ba_{4.5}Si_{46}$ composition is superconducting, and in ^{137}Ba NMR of this composition [75] a large Knight shift of 5930 ppm at 4.2 K was found, which is even larger than the shift for bulk Ba metal (4030 ppm). The large Knight shifts in the superconducing compositions [75,77] indicate that $g(E_f)$ includes a large peak, leading to the result that the relatively large T_c for these clathrates results from density of states features [78] rather than enhanced electron-phonon coupling due to low-energy vibrational states. Regarding the paramagnetism of the Na filler states, Reny et al. [79] prepared several low-filling Na_xSi_{136} samples and performed ^{23}Na NMR. The results showed that samples with $x < 8$, the dipolar interaction of the localized Na atoms broadens the lineshape while for $x > 8$ two narrow lines appear, explained by the weakening of dipolar effects and transition to metallicity. Later, He et al. [80] ascribed the ^{23}Na NMR broadening at low sodium concentration to randomly positioned vacant cages. Moreover, the temperature dependence of the Na_xSi_{136} and Na_xSi_{46} shifts were found to reflect the presence of pseudogaps at E_f, for which the activation energies are 37 meV and 105 meV, respectively. Note that recent work on $Ba_{8-x}Si_{46}$ and $Ba_8Al_7Si_{39}$ [81,82] assigned the largest ^{29}Si observed resonance lines to the 24*k* site in contrast to the earlier references. Finally note that for clathrates of composition $Si_{46-x}P_xTe_y$, ^{31}P NMR was also shown to give a broad line in the range of diamagnetic phosphorous [83].

Ge and Sn Clathrates: The Ge-based and Sn-based clathrates have larger cages compared to the Si-based, therefore, the rattler atoms can be off-centre and with greater anharmonicity for more effective reduction of the thermal conductivity. For example, single-crystal $Ba_8Ga_{16}Ge_{30}$ [84] was found to have an extrapolated zT = 1.63 at 1100 K. ^{69,71}Ga NMR has been studied for a number of systems, and Table 3 shows reported ^{71}Ga resonance shifts. In type-I compositions the spectra are quite broad, with an overlapping of the 3 framework sites typically making it difficult to extract Ga site occupations. However, a ($1/T_1$) analysis [85] as well as modeling of line shapes (Figure) have proved to be useful tools. Ga NMR line shapes and T_2 analysis for $Sr_8Ga_{16}Ge_{30}$ [86] indicated the presence of a very low energy activated process, and later results indicated [85] that Sr atom dynamics freeze below 50 K. Recently, Sirusi et al. [48] separated magnetic and quadrupole ($1/T_1$) contributions, showing that above room temperature the quadrupole term exceeds the classical T^2 process expected for itinerant phonons, an apparent indication of additional anharmonicity effects, possibly following the mechanism proposed for molecular crystals [87]. Ga and Sn NMR of the type-VIII $Ba_8Ga_{16}Sn_{30}$ structural variant [88] furthermore showed evidence for off-centre rattling of the type-VIII guests, while NMR results showing localized rattling in large-cage type-I $Ba_8Ga_{16}Sn_{30}$ were already described above (Figure). Chen *et al*. [89] and Sirusi *et al*. [90] also performed ^{63,65}Cu NMR measurements on $Ba_8Cu_xGe_{46-x}$ and on $Ba_8Cu_5Si_xGe_{41-x}$ extending to Si_{41} compositions. Based also on DFT modeling of Knight shifts, the results indicate a large change in

hybridization of band-edge states for Si-clathrate compositions, corresponding to the large upswing in Cu shifts as seen in Figure .

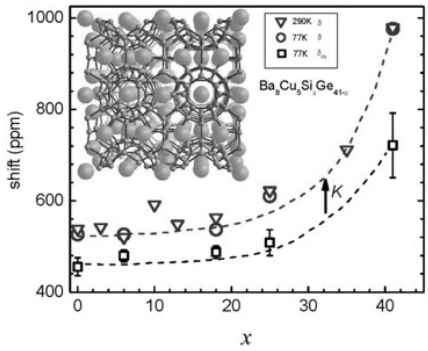

Figure 15: ^{63}Cu NMR chemical shifts for $Ba_8Cu_5Si_xGe_{41-x}$ at two temperatures shown, with 290 K Knight shift representing the difference between curves (arrow), with large change for Si clathrate compositions indicative of large change in metallicity. Reprinted with permission from [90], © 2015 the Owner Societies.

Other clathrates: Fulmer et al. [91] synthesized $Ba_8Au_{16}P_{30}$ with extremely low lattice thermal conductivity of 0.18W/m.K, in an orthorhombic variation of the cubic type-I structure. ^{31}P MAS NMR showed the presence of 3-fold bonded P sites and relatively large shifts. NMR studies of type-II Ge clathrate include ^{133}Cs NMR of Cs_8Ge_{136} [92] showing a large metallic shift (7600 ppm at RT) and the presence of Cs-Cs dimers between 343 and 384 K, with a pseudogap of 41 meV. However, no gap was found for $Cs_8Na_{16}Ge_{136}$, with a ^{133}Cs shift of –173 ppm [92]. NMR studies were also reported both for a H_2-encapsulating Si clathrate [93], and Li-intercalated Si clathrate [94].

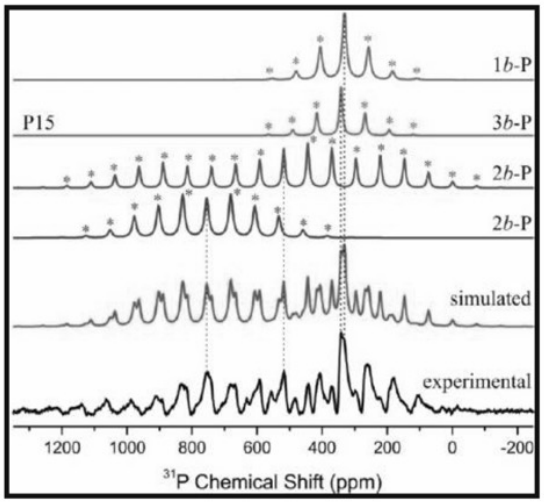

Figure 16: ^{31}P NMR of $Ba_8Au_{16}P_{30}$ showing four P sites, including 3-fold bonding configurations. Reprinted with permission from [91], © 2013 American Chemical Society.

Type-IX Ge-clathrate $Ba_{24}Ge_{100}$ has two transitions near 215, 180 K. ^{135,137}Ba and ^{73}Ge relaxation rates increase in the vicinity of 200 K due to the enhanced rattling of Ba associated with these transitions [95,96]. Moreover in a high-pressure NMR study [95], pressure-induced enhancement of $1/T_1$ in the low-T phase in 2.7 GPa provided confirmation of changes in $g(E_f)$ as the controlling mechanism for induced superconductivity.

Table 1: ^{29}Si NMR results for clathrate compounds. TMS = tetramethylsilane.

Compound	**Si sites**	**Resonance shifts (ppm)**	***T* (K)**	**Note**	**Std.**	**Ref.**
Na_4Si_{136}		618 845	300 K	Type II		[76]
$Na_{2.9}Ba_{4.5}Si_{46}$	16*i* 6*c* 24*k*	2036 862 720	90 K	Type I	TMS	[75]
Na_8Si_{46}	16*i* 6*c* 24*k*	617 653 842	300 K	Type I	TMS	[97]
$Na_{16}Cs_8Si_{136}$	8*a* 32*e* 96*g*	210 426 713	300 K	Type II	TMS	[98]
$Na_{19}Si_{136}$		1029	4.2 K	Type II		[99]
$Ba_8Ag_xSi_{46-x}$ (x=0~6)	–	–		Type I		[77]
Na_8Si_{46}	16*i* 6*c* 24*k*	613 648 840	300 K	Type I	TMS	[80]
$Na_{24}Si_{136}$	8*a* 32*e* 96*g*	 596 713	300 K	Type II		[80]
$Rb_8Na_{16}Si_{136}$	8*a* 32*e* 96*g*	275 420 735	300 K	Type II		[100]
Na_xSi_{136} (x = 0.0058)	8*a* 32*e* 96*g*	46.1 88.8 -3.6	300 K	Type II	TMS	[101]
$Ba_8Au_xSi_{46-x}$ (*x*=5.43, 5.89)	*x*=5.89: 200 ppm *x*=5.43: (600 ppm+		300 K	Type I		[102]

	0-1000 pm)			
$Ba_8B_{0.17}Al_{14}Si_{31}$	16*i*	-13	Type I	[103,104]
	6*c*	123		
	24*k*	204		
$Ba_8Al_{6.9}Si_{39.1}$	16*i*+6*c*	600	Type I	[82]
	24*k*	1100		
$Ba_{8-x}Si_{46}$	24k	1300-2200	Type I	[81]
	6c	770		
	16i	610		

Table 2 ^{23}Na NMR results for Si-based clathrates

Compound	**Na sites**	**resonance shifts (ppm)**	***T* (K)**	**Note**	**Std.**	**Ref.**
$Na_xBa_xSi_{46}$		1213		Type I	NaCl	[76]
Na_4Si_{136}	16*c*	1756		Type II	NaCl	[76]
	8*b*	2012				
Na_9Si_{136}	16*c*	1591		Type II	NaCl	[76]
	8*b*	1796				
$Na_{2.9}Ba_{4.5}Si_{46}$	2*a*	900	90 K	Type I	NaCl aq.	[75]
	6*d*					
$Na_{16}Cs_8Si_{136}$	16*c*	1738		Type II	NaCl	[98]
Na_8Si_{46}	16*c*	1601	300 K	Type I	NaCl aq.	[80]
	8*b*	1810				
$Na_{24}Si_{136}$	2a	2019	300 K	Type II		[80]
	6d	1768				
$Rb_8Na_{16}Si_{136}$	16c	1740	300 K	Type II		[100]

Table 3: Type I Ge and Sn clathrates, ^{71}Ga at room temperature with respect to Ga $(NO_3)_3$.

Compound	**^{71}Ga resonance shifts (ppm)**	**Ref.**
$Ba_8Ga_{16}Ge_{30}$	4478 (6*c*) 4509 (24*k*)	[105]
$Sr_8Ga_{16}Ge_{30}$	840	[86]
$Ba_8Ga_{16}Sn_{30}$	330	[56]
$Ba_8Ga_{16}Ge_{30}$	~490 (*n*-type) ~410 (*p*-type)	[85]
$Sr_8Ga_{16}Ge_{30}$	~490	[85]

2.2 Skutterudite compounds

Another important class of thermoelectric materials is filled skutterudites [106–108]. The structure of binary skutterudites is MX_3, where M represents transition metals Co, Fe, etc. and X is typically a pnictogen or chalcogenide. Figure 5 shows the structure, with 2 voids per cubic cell that can be occupied by filler atoms. Morelli and Meisner [109] showed that filler atoms reduce the thermal conductivity of $CeFe_4Sb_{12}$, after which Sales [110] and Fleurial [111] proposed applications in thermoelectric devices. There has since been a continued belief that anharmonic local vibrational properties will enhance such behavior, with the Sb-based skutterudites having particularly large voids for rattler atoms.

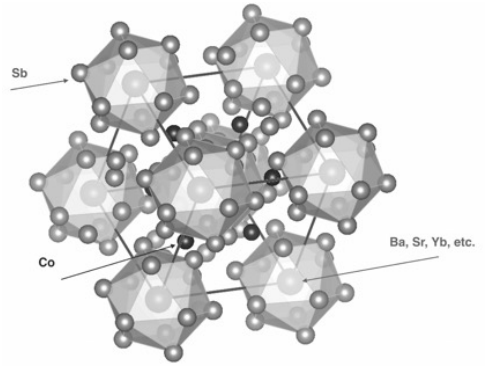

Figure 5: Filled skutterudite structure.

Recently there has been a large resurgence in interest for this application, since demonstration of large zT by multi-filling of $CoSb_3$. For example zT = 1.7 was reported at 850 K [112] through multi-filling by Ba, La, and Yb. $CoSb_3$ also has a very large power factor [106,108] so that nanostructuring or other means to reduce thermal conductiity may further enhance its zT. While filled $CoSb_3$ materials are normally n-type, to make p-type thermo-pairs filled $FeSb_3$, or mixed Fe-Sb compositions, are the most promising candidates. Thus although we have tabulated below references to a large number of NMR and NQR studies of filled skutterudite materials, in this review we have concentrated on the filled $CoSb_3$ and $FeSb_3$ materials of most direct interest for thermoelectric applications. Note however that it has also been proposed that $CoSb_3$ may be transformed into a topologically inverted material through small structural deformation [113], thus also leading to potential interest for spintronic or related applications. Also as was noted above, $YbFe_4Sb_{12}$ and related filled FeSb compositions exhibit heavy Fermion properties [39,46], and even with non-magnetic filler atoms $X Fe_4Sb_{12}$ materials exhibit other interesting magnetic properties.

In Table 4 we catergorized NMR and NQR results in filled skutterudites, including P-based, As-based, Ge-based, and Sb-based compounds. Note that a review of skutterudite magnetic behaviour is given in Ref. [114].

Table 4: NMR studies of filled skutterudites materials.

Compound	Resonance	Note	Reference
$LaRu_4P_{12}$	P NMR	Superconductor	[115]
$CeRu_4P_{12}$	P NMR	Semiconductor	[115,116]
$SmRu_4P_{12}$	P NMR	Metal-insulator transition	[117,118]
$EuRu_4P_{12}$	P NMR	Ferromagnetic	[119]
$GdRu_4P_{12}$	P NMR	Antiferromagnetic	[120]
$TbRu_4P_{12}$	P NMR	Antiferromagnetic	[120]
$Pr_{0.9}Ce_{0.1}Ru_4P_{12}$	P NMR	Metal-insulator transition	[121]
$NdRu_4P_{12}$	P NMR	Ferromagnetic	[122]
$LaFe_4P_{12}$	P NMR	Antiferromagnetic	[123]
UFe_4P_{12}	P NMR	Ferromagnetic	[124]
$CeFe_4P_{12}$	P NMR	Semiconductor	[116]
$GdFe_4P_{12}$	P NMR	Ferromagnetic	[125]
$TbFe_4P_{12}$	P NMR	Ferromagnetic	[125]
$PrFe_4P_{12}$	P NMR	Metal-Insulator	[126–130]
$YbFe_4P_{12}$	P NMR	Heavy Fermi-liquid	[131]
$NpFe_4P_{12}$	P NMR	Ferromagnetic	[132,133]
YFe_4P_{12}	P NMR	Superconductor	[134]
$LaOs_4P_{12}$	P NMR	Superconductor	[135]
$PrOs_4P_{12}$	P NMR	Superconductor	[135]
$NdOs_4P_{12}$	P NMR	Superconductor	[41]
$LaOs_4As_{12}$	La NMR	Multi-band superconductor	[136–138]
$LaFe_4As_{12}$	La NMR As-NQR	Multi-band superconductor	[139–141]
$CeFe_4As_{12}$	As-NQR	Kondo insulator	[141]
RPt_4Ge_{12} (R = La, Ce, Pr, Nd)	La NMR Pt-NMR	Superconductor	[142]
$LaPt_4Ge_{12}$	Ge-NMR/NQR	Superconductor	[143]
$PrPt_4Ge_{12}$ MPt_4Ge_{12}	Pt-NMR	Multi-band superconductor superconductors	[144]
$ThPt_4Ge_{12}$	Pt-NMR	Multi-band superconductor	[145]
$PrOs_4Sb_{12}$	Sb-NQR	superconductor	[146]
$PrRu_4Sb_{12}$	Sb-NQR	superconductor	[147]
$NaFe_4Sb_{12}$	Na-NMR Sb-NQR	Ferromagnetic	[148–150]
$LaFe_4Sb_{12}$	La-NMR Sb-NQR	Ferromagnetic	[150,151]
$CeOs_4Sb_{12}$	Sb-NMR	Ferromagnetic, Kondo insulating	[152]
$YbFe_4Sb_{12}$	Sb-NQR	Ferromagnetic	[51,131,151]

$La_{0.88}Fe_4Sb_{12}$	Sb-NQR	Ferromagnetic	[153]
(Ca,La)$CoSb_3$	Co-NMR	Semiconductor	[33,154,155]
AFe_4Sb_{12} (A= Ca, Sr, and Ba)	Sb-NQR	ferromagnetic	[156]
$CeFe_4Sb_{12}$	Sb-NQR	Semicondcutor	[157]
$LaOs_4Sb_{12}$	Sb-NQR La-NMR	Rattling	[55,158]
$SrFe_4Sb_{12}$ $CaFe_4Sb_{12}$	Sb-NQR	ferromagnetic pseudogap	[38]
$YbFe_4Sb_{12}$ $LaFe_4Sb_{12}$	Sb-NQR La-NMR	Intermediate valence, low thermal conductivity	[159]
$LaFe_4Sb_{12}$ $CaFe_4Sb_{12}$ $NaFe_4Sb_{12}$	Sb-NQR La-NMR Na-NMR	Displacemtnt of guest atoms pseudogap ferromagnetic	[22]
$CeOs_4Sb_{12}$	Sb-NMR	AFM	[160]
$PrOs_4Sb_{12}$	Sb-NMR	superconductor	[161]
MRu_4Sb_{12} (M=La,Ce, Pr)	Sb-NMR	Rattling	[162]
$CeOs_4Sb_{12}$	Sb-NQR	Ferromagnetic	[163]
$LaFe_4Sb_{12}$	Sb-NQR	Ferromagnetic	[164–166]
$CeFe_4Sb_{12}$ $La_{0.5}Co_4Sb_{12}$ $Sn_{0.4}Co_4Sb_{12}$ $Pr_{0.5}Co_4Sb_{12}$	La-NMR Sb-NQR La-NMR	Low thermal conductivity	[167]

$IrSb_3$, $CoSb_3$, and $CoAs_3$ have been predicted to have nearly linear dispersion at the band-edges [168], and as was noted above $CoSb_3$ may be quite close to topological inversion. The effect of a linear dispersion on the Seebeck coefficient gives a $p^{(-1/3)}$ behavior rather than the usual $p^{(-2/3)}$, in terms of hole density p, and the electrical conductivity would be proportional to $p^{(2/3)}$ instead p. Li *et al.* [169] by using *ab initio* calculations also predicted that $BaCoSb_3$ has low thermal conductivity due to anharmonicity throughout the phonon bands rather than due to localized rattling. Further NMR based local probes of the dynamical properties may be important to addresss the mechanism.

NMR measurements: ^{59}Co NMR results have been reported for (Ca,La)Co_4Sb_{12} [33,154,155], over a temperature range from 77K to 450 K. The line shapes have been found to be temperature independent, signs of non-magnetic behavior. However, with incorporation of the La and Ca atoms inside $CoSb_3$, it was also found that the line shapes become broader, a result attributed to random position of Ca or La inside the frameworks. The relaxation rates ($1/T_1$) vs T in all cases show activated features corresponding to narrow gaps at the Fermi level. This is shown in Figure(a) for $La_xCo_4Sb_{12}$ [154]. Knight shifts also show an increase vs T also characteristic of a narrow gap,

shown in Figure(b) for $La_xCo_4Sb_{12}$ [154] and in Figure for $Ca_xCo_4Sb_{12}$ [155]. The fitting function is $1/T_1T = 1/T_{1k}T + AT\,\mathrm{Exp}(-E_g/2k_BT)$ as described above for a pseudogap described as a residual density of states inside a semiconducting gap. The corresponding relation for K is $K_{iso}=K_0+A_1\sqrt{T}\,\mathrm{Exp}(-E_g/2k_BT)$.

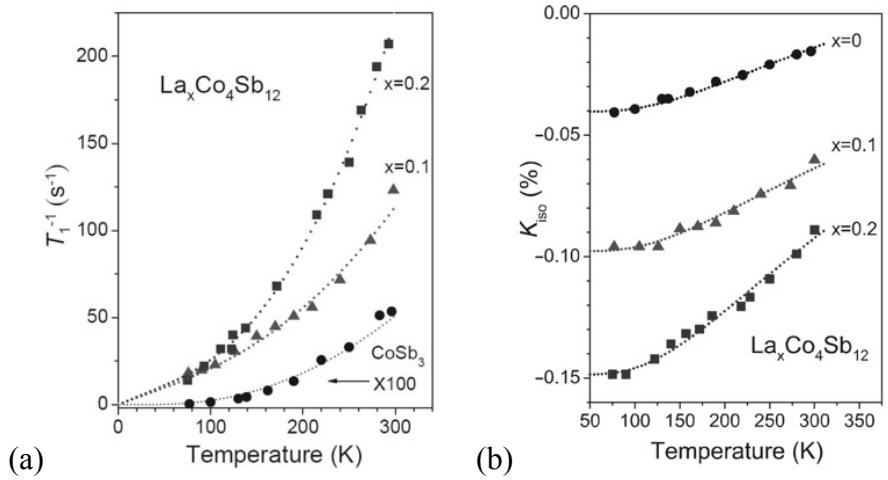

Figure 18: (a) $1/T_1$ vs T and, (b) K vs T, for Co NMR in $La_xCo_4Sb_{12}$. Reprinted with permission from [154], © 2008 IOP Publishing & Deutsche Physikalische Gesellschaft, CC BY-NC-SA.

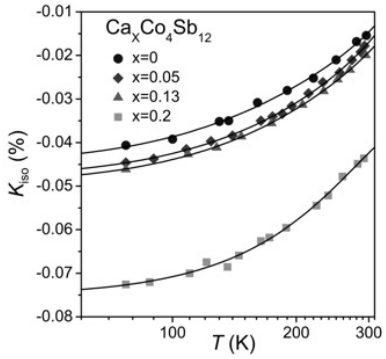

Figure 19: K vs T, for Co NMR in $Ca_xCo_4Sb_{12}$. Reprinted with permission from [155], © 2009 American Physical Society.

Fitting parameters are given in Table 5, including the quadrupole lineshape parameter ν_Q. Fitted gaps are surprisingly small, indicating a semimetallic overlap of bands with pseudogap, as compared to the semiconducting situation in unfilled $CoSb_3$. The overlap might be due to stabilization of electron pockets away from Γ, predicted [170] to contribute to the large power factor in filled $CoSb_3$ materials. As is seen, the factor $g(E_f)$ increases with both La and Ca filling.

Table 5: Filled $CoSb_3$ fitting parameters

Compound	E_g (meV)	ν_Q (MHz)	K_0 (%)	$1/T_{1K}T$ ($s^{-1}\,K^{-1}$)	$g(E_f)$ states/eV	Reference
$CoSb_3$	40	1.18	−0.042			[33]
$Ca_{0.05}Co_4Sb_{12}$	15	1.165	−0.048			[155]

$Ca_{0.13}Co_4Sb_{12}$	11	1.145	−0.049			[155]
$Ca_{0.2}Co_4Sb_{12}$	7	1.125	−0.075	0.079	0.51	[155]
$La_{0.1}Co_4Sb_{12}$	40	1.06	−0.098	0.194	0.794	[154]
$La_{0.2}Co_4Sb_{12}$	40	0.94	−0.148	0.218	0.844	[154]
$La_{0.5}Co_4Sb_{12}$		0				[167]
$Sn_{0.4}Co_4Sb_{12}$		1.14				[167]

It should be noted that for larger filling fraction, $La_{0.5}Co_4Sb_{12}$ synthesized under high pressure develops antiferromagnetic fluctuations, with $1/T_1T = C/(T+\theta)^{1/2}$ with θ = 30 K upon cooling [167], signaling even larger modifications of the electronic structure near E_f with filling. Significant differences have also been observed in the behavior of $Yb_xFe_4Sb_{12}$ samples at large filling fraction, as observed in NMR and NQR measurements [159]. For $La_xFe_4Sb_{12}$, NMR results indicating off-centre freezing of the filler atom were shown in Figure 3, and a low-temperature peak in $1/T_2$ was also reported [159] to indicate such a transformation.

2.3 Noble Metal Chalcogenides

As described in section 1.2.4, Cu_2Se recently has been subject of much interest for its potential for high-efficiency thermoelectric applications, with a large zT (1.5 at 1000 °C [17]) observed in the range of Cu hopping and superionic motion. For more detail on the superionic behaviour of Cu_2Se and related systems the reader can see [62,171]. Recent activity has focused on ways to harness the enhanced zT in superionic regime, or also perhaps to stabilize the ionic hopping in order to take advantage of the underlying semiconducting behavior. This class of materials includes several related materials of interest, also including CuAgSe, recently shown to have extermely high mobility perhaps due to Dirac-like electronic features [172] and potential for room temperature thermoelectric applications, Cu_2Te (see Figure), as well as corresponding sufides and Ag-based materials such as Ag_2Te. Aside from thermoelectric behavior, current interest in this class of materials also focuses on properties including topological behavior observed for example in Ag_2Te [173], and phase change devices which may utilize superionic-induced structure changes for next-generation memory applications [174].

NMR: ^{65,63}Cu NMR studies of Cu_2Se were described above as a probe of the development of ionic hopping, and eventually superionic motion at high temperatures [63–65]. Another issue for these materials is that the crystal structures are complex and in some cases unknown. Measurement of the NMR line shapes has helped to resolve these issues [65], for example the change in chemical shift at the superionic structural transition (Figure 6) was used to address questions of first order vs. second order phase transformation [175]. In addition, low temperature changes in Korringa behaviour [inset, Figure 4(b)] were found to be consistent with proposals of a low-temperature structure transformation [176].

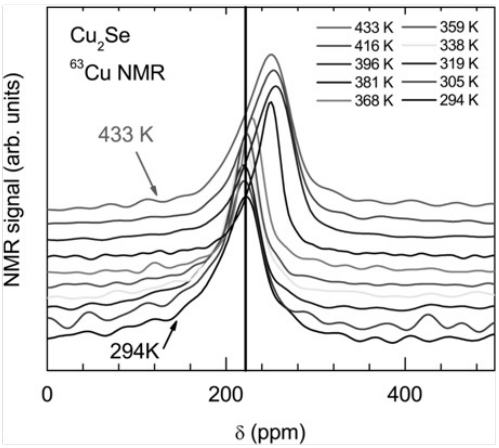

Figure 6: Evolution of ^{63}Cu motionally-narrowed NMR line near the Cu_2Se superionic structure transformation. Reprinted with permission from [65], © 2015 American Chemical Society.

In the case of $Cu_{2-x}Te$, a ^{63,65}Cu and ^{125}Te NMR study similarly focused on identifying the local site symmetries and electric field gradients, in comparison to proposed crystal superstructures [42]. As shown in Figure , that study also focused on the change of T_{1M} vs carrier density, as a means to understand the carrier-pocket properties of the band-structure, given that the structure is not fully understood. A previous study [43] study showed from analyzing the Korringa behavior that the p-type carriers include a very large Cu-site partial density of states $g_s(E_f)$. In addition by extrapolating the Korringa response (Figure), large negative chemical shifts were identified for both nuclei. This set of behavior has been associated with nontrivial topologically inverted band behavior. Cu-ion dynamics in Ag-substituted compositions were also addressed [43].

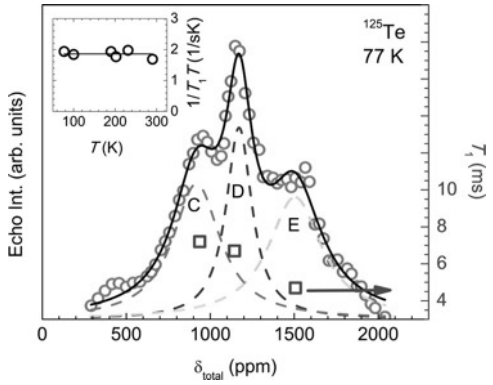

Figure 21: ^{125}Te NMR in Cu_2Te, with T_1 behavior shown overlayed demonstrating Korringa mechanism as dominating the differences in line position. Reprinted with permission from [43], © 2016 American Chemical Society.

The ^{63}Cu NMR was also studied for the high-mobility material CuAgSe [177]. In this case there is also a complicated crystal superstructure at low temperatures, and a superionic-induced structure transformation near 450 K. The Cu NMR lines are motionally narrowed above T_c, and progressively develop a much larger width in the low temperature static configuration. Figure shows the analysed widths, plotted also with the thermal conductivity, with the structural

transformation shown. This provides evidence that both the thermal conductivity and the linewidth are tied to the same phenomenon, thermally-activated hopping of Cu ions.

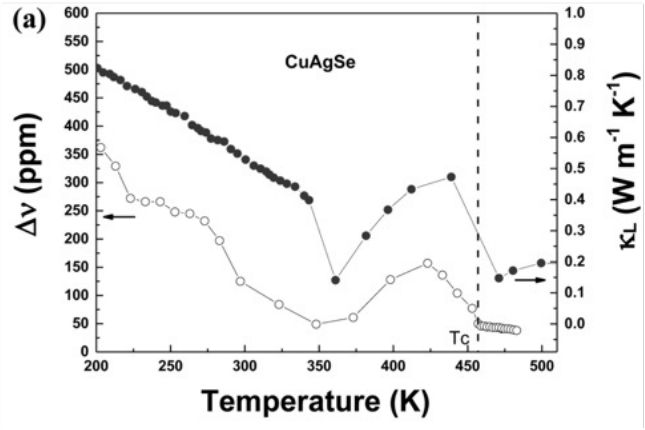

Figure 22: ^{63}Cu NMR linewidths measured in CuAgSe, vs temperature. Also shown in thermal conductivity, with the correlation between these results providing evidence for anharmonic phonon scattering from dynamic Cu ions. Reprinted with permission from [177], © 2016 American Chemical Society.

In CuAgS [178], a single motionally narrowed line was also observed above the structural transformation, with T_c near 380 K. As T_c is approached the linewidth increases, however for this case the line became unobservably broad for NMR detection below T_c. DFT-based calculations [178] also demonstrated the very large EFG's in the distorted low-temperature phase.

2.4 Oxide compounds

Oxide materials include a huge variety configurations, with many being of significant interest for potential applicability as thermoelectrics as well as fuel cells, photovoltaics, etc. [13,179]. While among these a number of oxide classes such as perovskites and delafossites have also been explored for potential thermoelectric application, here we describe specifically layered Co-based oxides which were shown to have a large power factor, generating considerable interest for thermoelectric applications. Na_xCoO_2 was first shown in 1997 [180] to have a large thermopower, leading to continuing interest in this material, which has a layered structure consisting of CoO_2 and Na-atom layers as shown in Figure . Depending on the Na content (x) there are four different structures, among which the compound close $x = 0.88$ shows maximum zT. The mechanism for the large thermopower is believed to be related the large spin entropy associated with Co-based d bands near E_f [181]. Similar oxide layered compounds Ca_3CoO_6 and $Bi_2M_2Co_{1.67}O_y$ (M = Ca, Sr, and Ba) also were discovered with values of zT comparable to those of the traditional thermoelectric materials. Figure shows the similarity of these structures with Na_xCoO_2. The Ca_3CoO_6 compound forms a misfit structure due to disorder in the Ca_2CoO_3 layers. While all of the above oxides have been reported to exhibit a large zT, they all are p-type, whereas for TE devices one also needs a compatible n-type thermoelectric leg. For this purpose, $SrTiO_3$ is found to be an excellent n-type compound if doped with Nb^{5+} and La^{3+} and represents one way these devices might be practical.

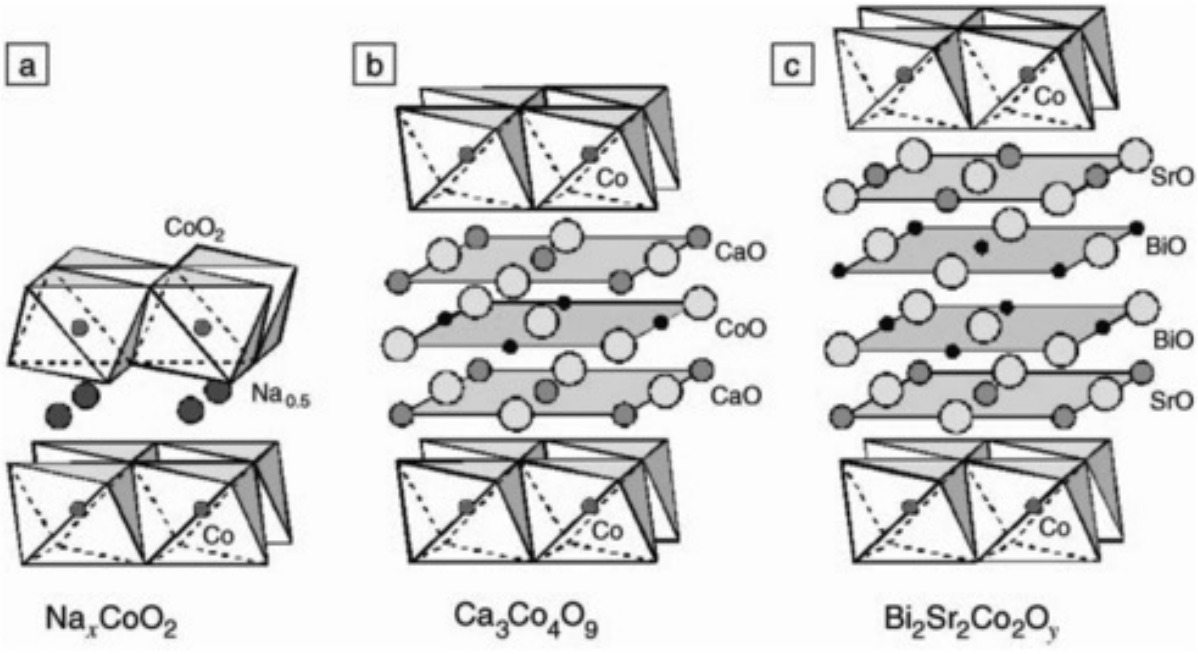

Figure 23: Structures of selected layered Co-oxide materials. Reprinted with permission from [182], © 2006 Materials Research Society.

Na_xCoO_2

As was mentioned, the physical properties of Na_xCoO_2 cobaltates are directly related to Na concentration (x); as x increases the doping decreases across a rich phase diagram. For $x < 0.5$ the material is a normal metal, for $x = 0.5$ an itinerant antiferromagnet and charge ordered insulator, for $x = 2/3$ a Curie-Weiss metal, and for $x = 1$ a band insulator. Thus, for $x > 0.5$ there is magnetic ordering, and a large number of NMR/NQR studies have addressed the magnetic and structural features of these phases. ^{23}Na and ^{59}Co NMR studies on $Na_{0.5}CoO_2$ cobaltate [183–191] have provided a great deal of information about the structure and the antiferromagnetic ($T = 87$ K) and metal insulator ($T = 53$ K) transitions. Bobroff et al. [183] assign the metal insulator transition to a SDW and later [186] report charge ordering as source of the metal insulator transition. As doping decreases the Na atoms become more ordered, while for $x > 0.75$ Na_xCoO_2 cobaltate has an A-type antiferromagnetic structure, in which the CoO_2 layers are ferromagnetic with an antiferromagnetic arrangement between planes [192–197]. Bobroff et al. [198] performed ^{59}Co NMR on several Bi misfit and Na cobaltates to single out the relation between magnetism and the large thermoelectricity. The Bi misfit samples have the same layer structure (CoO_2 alternating with rocksalt layers) with composition $[Bi_2M_2O_4]^{RS.}[CoO_2]_m$ (M = Ba, Sr, Ca, and m is the misfit ratio). Figure shows ^{59}Co NMR spectra of different samples. For low doping, Na atoms have more order hence less broadening, while incommensurability of the RS layers is the believed source of broadening for the misfit cobaltates. To further differentiate between these cobaltates the authors compared Seebeck coefficients and resistivity vs. shift parameters as shown in Figure 25. This showed that Na cobaltates have magnetic spin and charge ordering and are metallic for all doping, whereas they share only large thermoelectricity and Curie-Weiss susceptibility with Bi misfit cobaltates. Strong correlation is thus expected to be responsible for the large thermoelectric response in these materials.

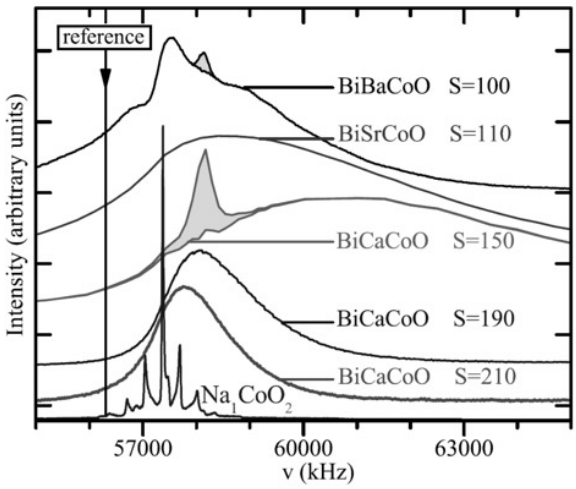

Figure 24: ^{59}Co NMR of misfit Bi cobaltates compared to $NaCoO_2$. Grey: Co_3O_4 contribution. Reprinted with permission from [198], © 2007 American Physical Society.

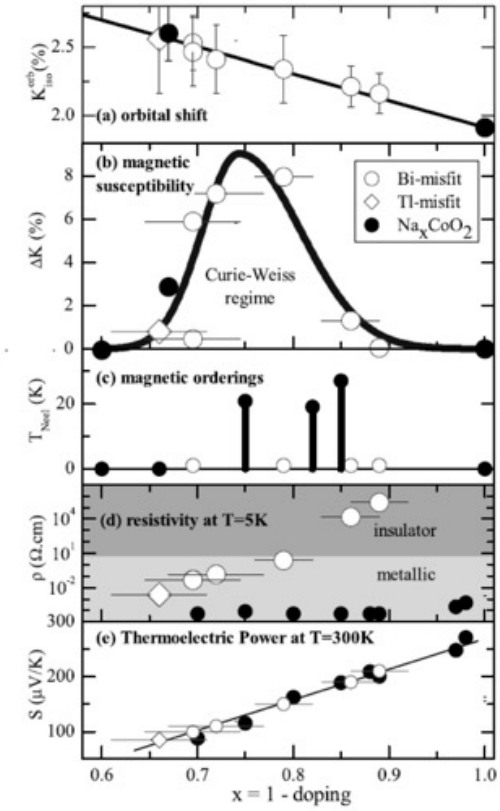

Figure 25: Comparison of (a) orbital Co NMR shift, (b) relative shift, (c) Neel temperature, (d) resistivity, (e) Seebeck coefficient, for cobaltate materials as shown. Reprinted with permission from [198], © 2007 American Physical Society.

$Ca_3Co_2O_6$

Several NMR studies were performed on $Ca_3Co_2O_6$ [199–202], all addressing the magnetic properties at low temperature, a frustrated Ising-type spin chain. In this compound Co atoms are in two spin states; high-spin Co^{3+} and nonmagnetic Co^{3+}. Sampathkumaran et al. [199] found a Co NMR signal below 15 K corresponding to non-magnetic cobalt sites. Shimizu [200] measured a single crystal, with Figure showing the angle dependence of the ^{59}Co spectra at room temperature. By applying a field parallel and perpendicular to the *c* axis, and comparing with the magnetic succeptibility they found parallel and perpendicular *K* parameters. Comparing to χ above 200 K these follow a Curie-Weiss law [$C/(T-\Theta)$] with Θ = 77 K for the field parallel, and Θ = -90 K perpenduclar to the *c* axis. These results were analysed to show the presense of intrachain ferromagnetic, and interchain antiferromagnetic coupling above 200 K. Measurements at 5 K in the ordered regime also pointed to a ferrimagnetic to ferromagnetic transition as a first-order transition. Later Allodi et al. [201,202] applied the NMR technique to extract more information about the magnetic properties, for example estimating the various exchange constants between sites.

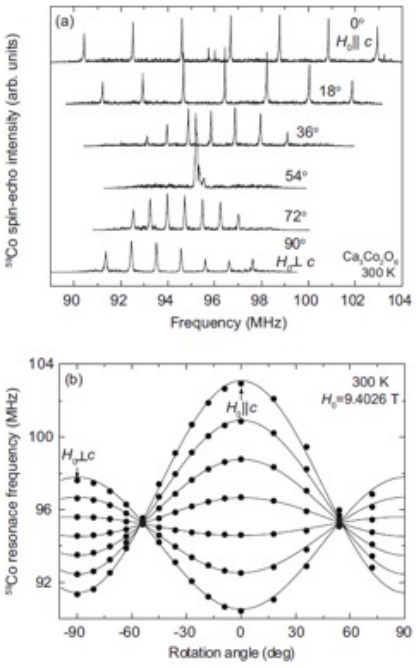

Figure 26: Orientation-dependent ^{59}Co NMR spectra for $Ca_3Co_2O_6$. Reprinted with permission from [200], © 2010 American Physical Society.

$[Ca_2CoO_3]_{0.62}CoO_2$ and $Ca_3Co_{3.92}O_{9.34-\delta}$ and $[Ca_2Co_{1.3}Cu_{0.7}O_4]_{0.62}CoO_2$:

$Ca_3Co_{3.92}O_{9.34-\delta}$ and $[Ca_2Co_{1.3}Cu_{0.7}O_4]_{0.62}CoO_2$ are also misfit cobaltates showing high thermoelectric efficiency. In addition, they have short- and long-range incommensurate spin-density wave (SDW) correlations below 100 K and 30 K, respectively, and a ferrimagnetic transition at 19 K, with CoO_2 layers responsible for the transport properties. Takami et al. [203,204] performed ^{59}Co NMR on $[Ca_2CoO_3]_{0.62}CoO_2$, $Ca_3Co_{3.92}O_{9.34-\delta}$ and

$[Ca_2Co_{1.3}Cu_{0.7}O_4]_{0.62}CoO_2$ at different temperature and different fields. They found 5 Co peaks, with two identified with the CoO_2 layer, indicating that the presence of two peaks is due to phase separation. Results showed that an SDW and ferromagnetism coexist the CoO_2 layer and can be controlled by the oxygen content (δ). From thermoelectric point of view, strong correlation here also play a role in enhancement of the Seebeck coefficient. A spin-state transition at 380 K will change the low-state Co^{4+} to the intermediate state in which entropy of 3*d* electrons will increase and in turn the Seebeck coefficient.

2.5 Bi, Pb, and Ge Tellurides.

Thermoelectrics based on PbTe, Bi_2Te_3, and GeTe and derivatives are well established as high efficiency materials for applications in the medium to low-temperature range. Figure 2 illustrates *zT* values for PbTe and Bi_2Te_3 as well as PbTeSe, and TAGS as shown in the figure denotes the series of Ag and Sb substituted GeTe themoelectrics, as was already mentioned in the introduction. Nanostructured derivatives of these materials can higher *zT* values, for example $zT = 1.8$ in melt spun *p*-type $Bi_{0.4}Sb_{1.6}Te_3$ [205], and $zT = 2.2$ in a nanoprecipitate $AgPb_{18}SbTe_{20}$ [206]. TAGS-85 denotes the composition $Ag_{6.52}Sb_{6.52}Ge_{36.96}Te_{50}$, and as recently reported, Dy doping in this material can enhance *zT* to > 1.5 [207], in which report NMR was used as a local measure of the carrier density.

Table 6 summarizes recent NMR studies focused upon understanding of complex thermoelectrics based on these materials. Among this work, Levin and colleagues have used NMR techniques to analyse local charge carrier properties in many different complex telluride thermoelectric systems, using ^{125}Te NMR as an analysis tool. For example, as noted above this was used to calibrate local carrier densities and effective masses in order to better understand the Seebeck response, and NMR has been used to detect large local variations in carrier behaviour in some of these materials. Figure shows a scaling relation for a series of GeTe-based materials [208], according to the Korringa relation $K^2T_1T =$ constant, and extrapolating to a common orbital shift (equivalent to the chemical shift as used here).

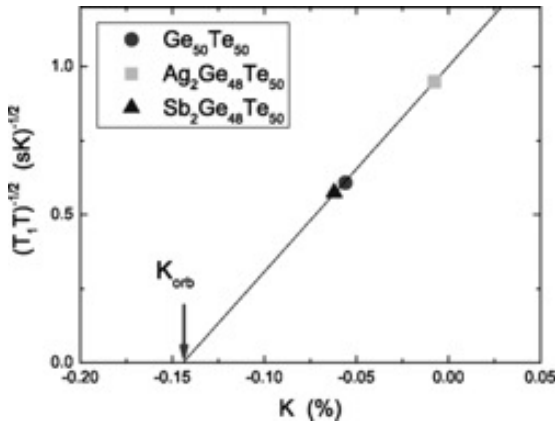

Figure 27: ^{125}Te $(T_1T)^{-1/2}$ plotted vs. *K* for a series of GeTe-based materials, with Korringa scaling showing extrapolation to common orbital shift. Reprinted with permission from [208], © 2016 American Physical Society.

Also as noted in the table, NMR measurements have also detected local phase segregation occurring in some of these materials, for example in rapidly quenched PbTe-PbS incipient phase separation was seen which could not be detected by synchrotron X-ray methods [209]. $Ag_{1-y}Pb_{18}Sb_{1+z}Te_{20}$ exhibited separation into two phases with an order of magnitude difference in carrier density [210].

In addition to this work, there has been much recent attention to fundamental properties of Bi_2Te_3, Bi_2Se_3, PbTe and PbSe via NMR measurements, with a large emphasis on probing the topological inversion and topological-insulator behaviour in these semiconducting materials. There has also been a focus on theoretical understanding of the spin-orbit effects on NMR shifts [211]. In Bi_2Te_3 a Te NMR study of nanoparticles showed development of a separate metallic peak in the small size limit [212], and a single crystal study showed a splitting into two phases, interpreted as evidence for surface peaks [213]. Synthesis dependent properties were also reported, including information on local antisite defects [214]. Pb NMR in PbSe showed electronic phase segregation into *n* and *p*-type regions [215], and in $Bi_2Te_{3-x}Se_x$ mixed conductivity at the ordered Bi_2Te_2Se composition was connected to local *n* and *p*-type regions through ^{125}Te NMR [216], and a correlation between the NMR shifts and sample conductivity also observed (Figure). Also in $Pb_{1-x}Sn_xTe$, ^{207}Pb, ^{119}Sn, and ^{125}Te NMR led to the conclusion that the topological band inversion in this material is associated with electronic inhomogeneities connected to the atomic sites having Sn substitution [217].

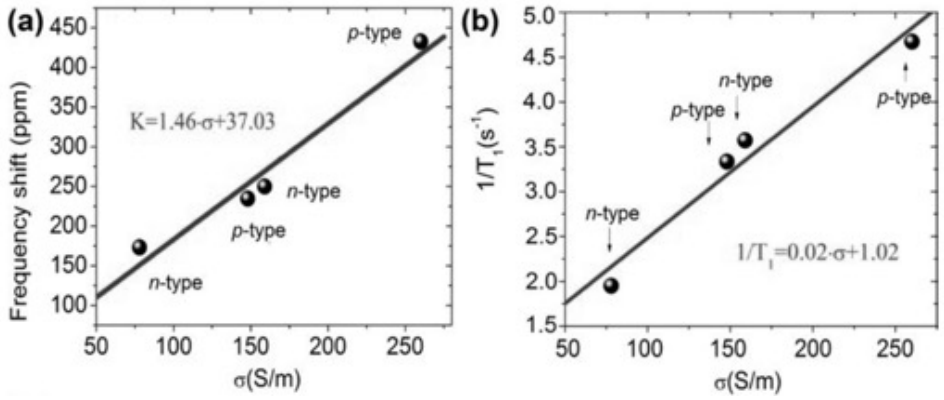

Figure 28: Correlation between ^{125}Te NMR shifts and conductivity in $Bi_2Te_{3-x}Se_x$ conductors. Reprinted from [216], © 2016 T. C. Chasapis, *et al*., Creative Commons Attribute (CC BY).

Table 6: NMR studies of thermoelectric telluride materials. TAGS-*x*, *x* denotes the GeTe fraction in a nominal $(GeTe)_x(AgSbTe_2)_{100-x}$ composition.

Year	Material	Nucleus	Note	Ref.
2009	Ag-Pb-Sb-Te	Te, Pb NMR	LAST-18 material; segregated 2-phase local electron density.	[210]
2011	AgSbGeTe, Ce- and Yb-Doped	Te NMR	TAGS-85; Diluted magnetic semiconductors; local carrier densities	[53]

2011	Ge–As–Sb–Te	Te NMR	Crystalline/glasses; 2-coordinated Te predominates. Random vacancy distribution in rocksalt configuration.	[218]
2012	AgSbGeTe, Dy doped	Te NMR	TAGS-85; local measure of carrier density.	[207]
2013	GeTe	Te NMR	NMR and transport measurements. probe of carrier configuration.	[219]
2013	AgSbGeTe-Dy_x alloys	Te NMR	Carrier distribution; enhancement of *zT* and entropy filtering.	[220]
2013	PbTe–PbS	Te NMR	Local probe of phase separation.	[209]
2014	Pb0.7Ge0.3Te and Pb0.5Ge0.5Te	Te NMR	Local probe of phase separation.	[221]
2016	GeTe-based materials, Te excess.	Te NMR	Korringa product over wide range of shifts, large local hole densities.	[222]
2016	GeTe, Ag-, Sb-substituted GeTe	Te NMR	2-band behaviour with pseudogap. Korringa scaling of *K* with composition	[208]
2016	GeTe, Ag and Sb substituted	Te NMR	Local charge carrier concentrations	[223]
2016	AgSbGeTe	Te NMR	TAGS-*x* materials; NMR as calibration of transport behaviour	[44]

2.6 Half-Heusler Compounds

Half-Heusler compounds with the general formula ABX have also been under extensive investigation for thermoelectric applications [224,225], with *zT* in the vicinity of 1 for some compositions as shown in Figure . In this case A and B are transition and noble metals and X is a metalloid [226,227]. These compounds form a cubic structure in the MgAgAs-type with space group *F-43m* (Figure). As already described for CoTiSb (Figure), a number of compositions are semiconducting or nearly semiconducting, and it is materials based on these compositions that are generally targeted for thermoelectric application. Related materials in the half-Heusler alloy system are also subject of active interest due to other interesting features, such as strongly correlated electrons or topological insulator behaviour [228–230].

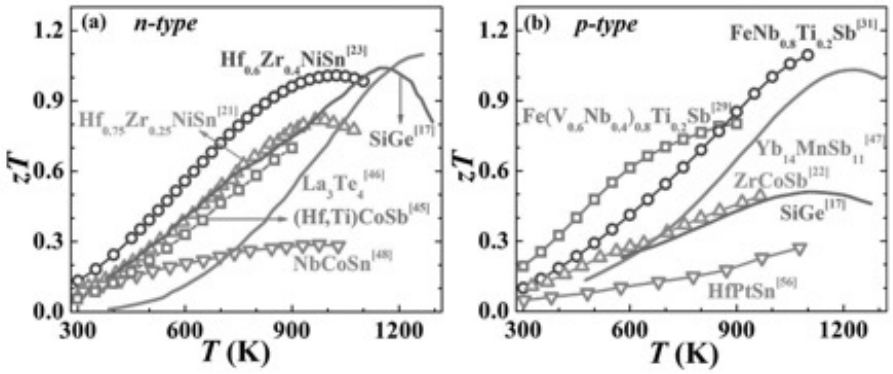

Figure 29: *zT* comparison of thermoelectric materials including (Hf,Zr)NiSn and FeNbSb based half-Heusler materials. Reprinted with permission from [227], © 2015 WILEY-VCH Verlag GmbH & Co. KGaA, Weinheim.

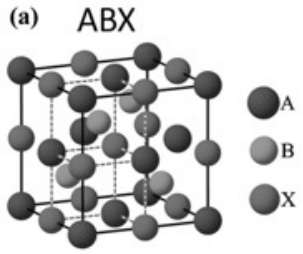

Figure 30: Half-Heusler ABX structure. Reprinted with permission from [227], © 2015 WILEY-VCH Verlag GmbH & Co. KGaA, Weinheim.

NMR studies: Several references to NMR study of these materials were given in the foregoing, addressing in particular local electronic features relating to semiconductor or pseudogap behaviour. Many additional recent work has focused on magnetic and topological properties of the materials. A summary of recent NMR work is given in Table 7.

Table 7: Summary of recent NMR studies of half-Heusler materials.

Year	Material	Nucleus	Note	Ref.
2001	FeVSn and CoVSn	^{51}V NMR	magnetic	[231]
2005	MPtSn (M=Ti, Zr, Hf, Th)	^{47,49}Ti, ^{91}Zr NMR	Diamagnetic; structural order/disorder	[232]
2005	MPtSn semiconductors (M = Ti, Zr, Hf, Th)	^{119}Sn, ^{195}Pt NMR	indirect spin coupling between Pt and Sn nuclei	[233]
2006	CoVSn	Zero field NMR	Proposed half-metallic ferromagnet	[234]
2006	UPtSn	^{119}Sn and ^{195}Pt NMR	Orbital ordering	[235]

2006	CoMnSb	Mn, Sb	Proposed half-metallic ferromagnet	[236]
2007	TiPtSn and ZrPtSn	^{195}Pt NMR	semiconductors	[52]
2008	UPtSn and ThPtSn	^{119}Sn , ^{195}Pt NMR	Transfer hyperfine coupling; narrow gap, spin dynamics	[237]
2009	CoTiSb	^{59}Co NMR	pseudogap	[31]
2009	Sc*T*Sb (*T* = Ni, Pd, Pt)	^{45}Sc MAS NMR	Spectral splitting/vacancy formation	[238]
2011	YbPtSb and LuPtSb	$^{121/123}$Sb, ^{195}Pt NMR	Magnetic fluctuations, local moments	[239]
2013	YPdSb, YPtSb and LuPtSb	^{121,123}Sb	Phonon relaxation processes	[240]
2014	LiTX (T = Mg, Zn, Cd; X = P, As, Sb, Bi)	^{7}Li, ^{25}Mg, ^{113}Cd, ^{31}P, ^{75}As, ^{121}Sb NMR	Bonding trends; Li-ion mobility.	[241]
2014	YPdBi and YPtBi	^{209}Bi NMR	Topological inversion	[228]
2015	MgAgSb	Mg NMR	High *zT*; ion mobility	[67]
2015	ScPdBi, LuPdBi, and LuPtBi	^{209}Bi NMR	Topological inversion	[242]
2015	YPdBi and YPtBi	^{209}Bi NMR	Topological inversion	[229]
2016	*T*Pt*X* (*T* = Ti, Zr, Hf, *X* = Si, Ge), TiPtSn	^{29}Si, ^{47,49}Ti, ^{195}Pt MAS NMR	Structure change	[243]
2016	ScPtBi, LaPdBi, and LaPtBi.	^{209}Bi NMR	Topological inversion	[244]
2016	*RM*Bi, *R*=Sc, Y, Lu; *M*=Pd,Pt, Ni	^{209}Bi NMR	Topological inversion	[230]

Conclusions

Recent NMR measurements have been surveyed for several classes of inorganic thermoelectric materials of current interest. These measurements address a number of features which are of significance in optimizing thermoelectric efficiency, including anharmonic and inhomogeneous vibrational behaviour, local fluctuations in charge carrier and magnetic properties, and atomic-scale symmetries and phase segragation. This survey focus on materials including inorganic clathrates, skutterudites, cobalt oxides, noble metal chalcogenides, complex tellurides, and half-

Huesler compounds, in which families high thermoelectric efficiencies have been reported. In addition NMR concepts of particlular relevance to these thermoelectric materials are reviewed.

Acknowledgements

This work was supported by the Robert A. Welch Foundation, Grant No. A-1526.

References

[1] X. Shi, L. Chen, C. Uher, Recent advances in high-performance bulk thermoelectric materials, Int. Mater. Rev. 61 (2016) 379–415. doi:10.1080/09506608.2016.1183075.

[2] A. V. Shevelkov, Chemical aspects of the design of thermoelectric materials, Russ. Chem. Rev. 77 (2008) 1–19. doi:10.1070/RC2008v077n01ABEH003746.

[3] H. Kleinke, New bulk Materials for Thermoelectric Power Generation: Clathrates and Complex Antimonides, Chem. Mater. 22 (2010) 604–611. doi:10.1021/cm901591d.

[4] M. Zebarjadi, K. Esfarjani, M.S. Dresselhaus, Z.F. Ren, G. Chen, Perspectives on thermoelectrics: from fundamentals to device applications, Energy Environ. Sci. 5 (2012) 5147–5162. doi:10.1039/C1EE02497C.

[5] T.M. Tritt, Thermoelectric Phenomena, Materials, and Applications, Annu. Rev. Mater. Res. 41 (2011) 433–448. doi:10.1146/annurev-matsci-062910-100453.

[6] J.H. Ross, Y. Li, Superconductivity and Magnetism in Silicon and Germanium Clathrates, in: Nanoscale Magn. Mater. Appl., Springer US, Boston, MA, 2009: pp. 105–122. doi:10.1007/978-0-387-85600-1_4.

[7] T.J. Seebeck, Magnetische polarisation der metalle und erze durch temperatur-differenz, Abh. K. Akad. Wiss. Berlin. (1823) 265.

[8] T.J. Seebeck, Ueber die magnetische Polarisation der Metalle und Erze durch Temperaturdifferenz, Ann. Phys. 82 (1826) 253.

[9] J.C. Peltier, Nouvelles experiences sur la caloricité des courants electrique, Ann. Chim. Phys. 56 (1834) 371.

[10] G.J. Snyder, E.S. Toberer, Complex thermoelectric materials., Nat. Mater. 7 (2008) 105–114. doi:10.1038/nmat2090.

[11] Y. Pei, X. Shi, A. LaLonde, H. Wang, L. Chen, G.J. Snyder, Convergence of electronic bands for high performance bulk thermoelectrics, Nature. 473 (2011) 66–69. doi:10.1038/nature09996.

[12] Q. Zhang, H. Wang, W. Liu, H. Wang, B. Yu, Q. Zhang, Z. Tian, G. Ni, S. Lee, K. Esfarjani, G. Chen, Z. Ren, Enhancement of thermoelectric figure-of-merit by resonant states of aluminium doping in lead selenide, Energy Environ. Sci. 5 (2012) 5246–5251. doi:10.1039/C1EE02465E.

[13] P. Brinks, M. Huijben, Thermoelectric oxides, in: Ep. Growth Complex Met. Oxides, Elsevier, 2015: pp. 397–441. doi:10.1016/B978-1-78242-245-7.00014-2.

[14] L. Wu, J. Yang, S. Wang, P. Wei, J. Yang, W. Zhang, L. Chen, Two-dimensional thermoelectrics with Rashba spin-split bands in bulk BiTeI, Phys. Rev. B. 90 (2014) 195210. doi:10.1103/PhysRevB.90.195210.

[15] T. Takabatake, K. Suekuni, T. Nakayama, E. Kaneshita, Phonon-Glass Electron-Crystal Thermoelectric Clathrates: Experiments and Theory, Rev. Mod. Phys. 86 (2014) 669–716. doi:10.1103/RevModPhys.86.669.

[16] L.-D. Zhao, S.-H. Lo, Y. Zhang, H. Sun, G. Tan, C. Uher, C. Wolverton, V.P. Dravid, M.G. Kanatzidis, Ultralow thermal conductivity and high thermoelectric figure of merit in SnSe crystals., Nature. 508 (2014) 373–7. doi:10.1038/nature13184.
[17] H. Liu, X. Shi, F. Xu, L. Zhang, W. Zhang, L. Chen, Q. Li, C. Uher, T. Day, G.J. Snyder, Copper ion liquid-like thermoelectrics, Nat. Mater. 11 (2012) 422–425. doi:10.1038/nmat3273.
[18] M.W. Gaultois, T.D. Sparks, C.K.H. Borg, R. Seshadri, W.D. Bonificio, D.R. Clarke, Data-Driven Review of Thermoelectric Materials: Performance and Resource Considerations, Chem. Mater. 25 (2013) 2911–2920. doi:10.1021/cm400893e.
[19] K. Schwarz, DFT calculations of solids with LAPW and WIEN2k, J. Solid State Chem. 176 (2003) 319–328. doi:10.1016/S0022-4596(03)00213-5.
[20] W. Gou, S. Rodriguez, Y. Li, J. Ross, NMR experiments and electronic structure calculations in type-I BaAlGe clathrates, Phys. Rev. B. 80 (2009) 144108. doi:10.1103/PhysRevB.80.144108.
[21] S.Y. Rodriguez, X. Zheng, L. Saribaev, J.H. Ross, NMR and Computational Studies of Ba8Ga16Sn30 Clathrates, MRS Proc. 1267 (2010) 1267-DD04-7. doi:10.1557/PROC-1267-DD04-07.
[22] A.A. Gippius, K.S. Okhotnikov, A. V. Shevel'kov, Static displacement of a guest atom in filled skutterudites MFe4Sb12 (M = La, Ca, Na), JETP Lett. 89 (2009) 200–204. doi:10.1134/S0021364009040080.
[23] T. Charpentier, The PAW/GIPAW approach for computing NMR parameters: A new dimension added to NMR study of solids, Solid State Nucl. Magn. Reson. 40 (2011) 1–20. doi:10.1016/j.ssnmr.2011.04.006.
[24] V. Baran, A. Senyshyn, A.J. Karttunen, A. Fischer, W. Scherer, G. Raudaschl-Sieber, T.F. Fässler, A Combined Metal-Halide/Metal Flux Synthetic Route towards Type-I Clathrates: Crystal Structures and Thermoelectric Properties of A8Al8Si38 (A=K, Rb, and Cs), Chem. - A Eur. J. 20 (2014) 15077–15088. doi:10.1002/chem.201403416.
[25] R.E. Taylor, F. Alkan, D. Koumoulis, M.P. Lake, D. King, C. Dybowski, L.-S. Bouchard, A Combined NMR and DFT Study of Narrow Gap Semiconductors: The Case of PbTe, J. Phys. Chem. C. 117 (2013) 8959–8967. doi:10.1021/jp3101877.
[26] G.C. Carter, L.H. Bennett, D.J. Kahan, Knight shifts in alloys and intermetallic compounds, Prog. Mater. Sci. 20 (1976) 22–41. doi:10.1016/0079-6425(76)90034-7.
[27] D. Wolf, Spin Temperature and Nuclear Spin Relaxation in Matter: Basic Principles and Applications, First Edit, Oxford, Clarendon, 1979.
[28] J. Lu, M.J.R. Hoch, P.L. Kuhns, W.G. Moulton, Z. Gan, A.P. Reyes, Nuclear spin-lattice relaxation in n-type insulating and metallic GaAs single crystals, Phys. Rev. B. 74 (2006) 125208. doi:10.1103/PhysRevB.74.125208.
[29] M.A. Paalanen, A.E. Ruckenstein, G.A. Thomas, Spins in Si: P Close to the Metal-Insulator Transition, Phys. Rev. Lett. 54 (1985) 1295–1298. doi:10.1103/PhysRevLett.54.1295.
[30] N. Roberts, R.-P. Wang, A.W. Sleight, W.W. Warren, 27Al and 69Ga impurity nuclear magnetic resonance in ZnO:Al and ZnO:Ga, Phys. Rev. B. 57 (1998) 5734–5741. doi:10.1103/PhysRevB.57.5734.
[31] C. Lue, C. Chen, F.-K. Chiang, M.-W. Chu, Annealing effect on the reduction of Fermi-level density of states in CoTiSb: NMR evidence, Phys. Rev. B. 80 (2009) 174202. doi:10.1103/PhysRevB.80.174202.

[32] G.S. Tripathi, L.K. Das, P.K. Misra, S.D. Mahanti, Theory of spin-orbit and many-body effects on the Knight shift, Phys. Rev. B. 25 (1982) 3091–3116. doi:10.1103/PhysRevB.25.3091.
[33] C.S. Lue, Y.T. Lin, C.N. Kuo, NMR investigation of the skutterudite compound CoSb3, Phys. Rev. B. 75 (2007) 75113. doi:10.1103/PhysRevB.75.075113.
[34] R. Laskowski, P. Blaha, NMR Shielding in Metals Using the Augmented Plane Wave Method, J. Phys. Chem. C. 119 (2015) 19390–19396. doi:10.1021/acs.jpcc.5b05947.
[35] J.J. van der Klink, H.B. Brom, NMR in Metals, Metal Particles and Metal Cluster Compounds, Prog. Nucl. Magn. Reson. Spectrosc. 36 (2000) 89–201. doi:10.1016/s0079-6565(99)00020-5.
[36] R.K. Sundfors, D.F. Holcomb, Nuclear Magnetic Resonance Studies of the Metallic Transition in Doped Silicon, Phys. Rev. 136 (1964) A810–A820. doi:10.1103/PhysRev.136.A810.
[37] J.P. Yesinowski, Solid-State NMR of Inorganic Semiconductors, in: Top. Curr. Chem., Springer Berlin Heidelberg, 2011: pp. 229–312. doi:10.1007/128_2011_208.
[38] A. Sakurai, M. Matsumura, H. Kato, T. Nishioka, E. Matsuoka, K. Hayashi, T. Takabatake, Low-field Knight shift measurement at Sb site for alkaline-earth filled skutterudites AFe4Sb12 (A = Sr and Ca), J. Phys. Soc. Japan. 77 (2008) 63701. doi:10.1143/JPSJ.77.063701.
[39] W. Schnelle, A. Leithe-Jasper, H. Rosner, R. Cardoso-Gil, R. Gumeniuk, D. Trots, J.A. Mydosh, Y. Grin, Magnetic, thermal, and electronic properties of iron-antimony filled skutterudites MFe4Sb12 (M = Na,K,Ca,Sr,Ba,La,Yb), Phys. Rev. B. 77 (2008) 94421. doi:10.1103/PhysRevB.77.094421.
[40] M.J.R. Hoch, D.F. Holcomb, 31P Knight Shifts and Spin Dynamics in Si:P at Temperatures Comparable to the Fermi Temperature, Phys. Rev. B. 71 (2005) 35115. doi:10.1103/PhysRevB.71.035115.
[41] K. Magishi, K. Nagata, Y. Iwahashi, H. Sugawara, T. Saito, K. Koyama, NMR study of filled skutterudite NdOs4P12, J. Phys. Conf. Ser. 200 (2010) 12110. doi:10.1088/1742-6596/200/1/012110.
[42] A.A. Sirusi, A. Page, C. Uher, J.H. Ross, NMR study of vacancy and structure-induced changes in Cu2-xTe, J. Phys. Chem. Solids. 106 (2017) 52–57. doi:10.1016/j.jpcs.2017.02.016.
[43] A.A. Sirusi, S. Ballikaya, J.-H. Chen, C. Uher, J.H. Ross, Band Ordering and Dynamics of Cu2–xTe and Cu1.98Ag0.2Te, J. Phys. Chem. C. 120 (2016) 14549–14555. doi:10.1021/acs.jpcc.6b04785.
[44] E.M. Levin, Charge carrier effective mass and concentration derived from combination of Seebeck coefficient and 125Te NMR measurements in complex tellurides, Phys. Rev. B. 93 (2016) 245202. doi:10.1103/PhysRevB.93.245202.
[45] J.P. Heremans, B. Wiendlocha, A.M. Chamoire, Resonant levels in bulk thermoelectric semiconductors, Energy Environ. Sci. 5 (2012) 5510–5530. doi:10.1039/C1EE02612G.
[46] S. V. Dordevic, D.N. Basov, N.R. Dilley, E.D. Bauer, M.B. Maple, Hybridization Gap in Heavy Fermion Compounds, Phys. Rev. Lett. 86 (2001) 684–687. doi:10.1103/PhysRevLett.86.684.
[47] C.S. Lue, J.H. Ross, Pseudogap in Fe2VGa: NMR evidence, Phys. Rev. B. 63 (2001) 54420. doi:10.1103/PhysRevB.63.054420.
[48] A.A. Sirusi, J.H. Ross, Pseudogap and anharmonic phonon behavior in Ba8Ga16Ge30: An

NMR study, J. Chem. Phys. 145 (2016) 54702. doi:10.1063/1.4960054.
[49] J. Winter, Magnetic resonance in metals, Clarendon, Oxford, 1971.
[50] R.E. Walstedt, The NMR Probe of High-Tc Materials, Springer Berlin Heidelberg, 2008. doi:10.1007/978-3-540-75565-4.
[51] K. Magishi, R. Watanabe, A. Hisada, T. Saito, K. Koyama, Pseudogap Behavior in Fully Filled Skutterudite YbFe4Sb12 Detected by Sb NQR, J. Phys. Soc. Japan. 83 (2014) 84712. doi:10.7566/JPSJ.83.084712.
[52] a. Grykałowska, B. Nowak, Nuclear spin-lattice relaxation in narrow gap semiconductors TiPtSn and ZrPtSn, Intermetallics. 15 (2007) 1479–1482. doi:10.1016/j.intermet.2007.05.009.
[53] E.M. Levin, B. a. Cook, J.L. Harringa, S.L. Bud'ko, R. Venkatasubramanian, K. Schmidt-Rohr, Analysis of Ce- and Yb-Doped TAGS-85 Materials with Enhanced Thermoelectric Figure of Merit, Adv. Funct. Mater. 21 (2011) 441–447. doi:10.1002/adfm.201001307.
[54] J.P. Yesinowski, Finding the true spin–lattice relaxation time for half-integral nuclei with non-zero quadrupole couplings, J. Magn. Reson. 252 (2015) 135–144. doi:10.1016/j.jmr.2014.12.012.
[55] Y. Nakai, K. Ishida, H. Sugawara, D. Kikuchi, H. Sato, Low-lying excitations at the rare-earth site due to the rattling motion in the filled skutterudite LaOs4Sb12 revealed by 139La NMR and 121/123Sb NQR, Phys. Rev. B. 77 (2008) 41101. doi:10.1103/PhysRevB.77.041101.
[56] X. Zheng, S.Y. Rodriguez, J.H. Ross, NMR relaxation and rattling phonons in the type-I Ba8Ga16Sn30 clathrate, Phys. Rev. B. 84 (2011) 24303. doi:10.1103/PhysRevB.84.024303.
[57] H. Tou, K. Sonoda, K. Furumoto, H. Kotegawa, K. Suekuni, M. A. Avila, T. Takabatake, Strong Coupling of Rattling Phonon to Conduction Electrons in Semimetallic Type-I Clathrate Ba8Ga16Sn30, J. Phys. Soc. Japan. 82 (2013) 114603. doi:10.7566/JPSJ.82.114603.
[58] T. Dahm, K. Ueda, NMR Relaxation and Resistivity from Rattling Phonons in Pyrochlore Superconductors, Phys. Rev. Lett. 99 (2007) 187003. doi:10.1103/PhysRevLett.99.187003.
[59] Y. Kasahara, Y. Shimono, T. Shibauchi, Y. Matsuda, S. Yonezawa, Y. Muraoka, Z. Hiroi, Thermal Conductivity of the Pyrochlore Superconductor KOs2O6 : Strong Electron Correlations and Fully Gapped Superconductivity, Phys. Rev. Lett. 96 (2006) 247004. doi:10.1103/PhysRevLett.96.247004.
[60] P. Thalmeier, Anharmonic effects in the mixed 4f-electron lattice excitations of Pr skutterudites, Phys. Rev. B - Condens. Matter Mater. Phys. 83 (2011) 195124. doi:10.1103/PhysRevB.83.195124.
[61] C.P. Grey, N. Dupré, NMR Studies of Cathode Materials for Lithium-Ion Rechargeable Batteries, Chem. Rev. 104 (2004) 4493–4512. doi:10.1021/cr020734p.
[62] D. Brinkmann, NMR studies of superionic conductors, Prog. Nucl. Magn. Reson. Spectrosc. 24 (1992) 527–552. doi:10.1016/0079-6565(92)80009-5.
[63] T. Kanashiro, T. Ohno, M. Satoh, K. Okamoto, A. Kojima, F. Akao, Nuclear magnetic resonance and electrical conduction of copper chalcogenides, Solid State Ionics. 3–4 (1981) 327–330. doi:10.1016/0167-2738(81)90107-7.
[64] T. Kanashiro, NMR study of mobile ions in CuxSe and CuxS, Solid State Ionics. 40–41 (1990) 308–311. doi:10.1016/0167-2738(90)90347-T.

[65] A.A. Sirusi, S. Ballikaya, C. Uher, J.H. Ross, Low-Temperature Structure and Dynamics in Cu2Se, J. Phys. Chem. C. 119 (2015) 20293–20298. doi:10.1021/acs.jpcc.5b06079.
[66] W.G. Zeier, C.P. Heinrich, T. Day, C. Panithipongwut, G. Kieslich, G. Brunklaus, G.J. Snyder, W. Tremel, Bond strength dependent superionic phase transformation in the solid solution series Cu2ZnGeSe4−xSx, J. Mater. Chem. A. 2 (2014) 1790–1794. doi:10.1039/C3TA13007J.
[67] D. Li, H. Zhao, S. Li, B. Wei, J. Shuai, C. Shi, X. Xi, P. Sun, S. Meng, L. Gu, Z. Ren, X. Chen, Atomic Disorders Induced by Silver and Magnesium Ion Migrations Favor High Thermoelectric Performance in α-MgAgSb-Based Materials, Adv. Funct. Mater. 25 (2015) 6478–6488. doi:10.1002/adfm.201503022.
[68] Rogl, Formation and Crystal Chemistry of Clathrates, in: Thermoelectr. Handb., CRC Press, 2005: pp. 32-1-32–24. doi:10.1201/9781420038903.ch32.
[69] J.-A. Dolyniuk, B. Owens-Baird, J. Wang, J. V. Zaikina, K. Kovnir, Clathrate thermoelectrics, Mater. Sci. Eng. R Reports. 108 (2016) 1–46. doi:10.1016/j.mser.2016.08.001.
[70] G. Slack, New Materials and Performance Limits for Thermoelectric Cooling, in: CRC Handb. Thermoelectr., CRC Press, 1995: pp. 407–437. doi:10.1201/9781420049718.ch34.
[71] G.S. Nolas, ed., The Physics and Chemistry of Inorganic Clathrates, Springer Netherlands, 2014. doi:10.1007/978-94-017-9127-4.
[72] K. Suekuni, M.A. Avila, K. Umeo, T. Takabatake, Cage-size control of guest vibration and thermal conductivity in Sr8Ga16Si30−xGex, Phys. Rev. B. 75 (2007) 195210. doi:10.1103/PhysRevB.75.195210.
[73] S. Pailhès, H. Euchner, V.M. Giordano, R. Debord, A. Assy, S. Gomès, A. Bosak, D. Machon, S. Paschen, M. de Boissieu, Localization of Propagative Phonons in a Perfectly Crystalline Solid, Phys. Rev. Lett. 113 (2014) 25506. doi:10.1103/PhysRevLett.113.025506.
[74] M. Pouchard, C. Cros, P. Hagenmuller, E. Reny, A. Ammar, M. Ménétrier, J.-M. Bassat, A brief overview on low sodium content silicides: are they mainly clathrates, fullerenes, intercalation compounds or Zintl phases?, Solid State Sci. 4 (2002) 723–729. doi:10.1016/S1293-2558(02)01319-5.
[75] F. Shimizu, Y. Maniwa, K. Kume, H. Kawaji, S. Yamanaka, M. Ishikawa, NMR study in the superconducting silicon clathrate compound NaxBaySi46, Phys. Rev. B. 54 (1996) 13242–13246. doi:10.1103/PhysRevB.54.13242.
[76] J. Gryko, P. McMillan, O. Sankey, NMR studies of Na atoms in silicon clathrate compounds., Phys. Rev. B Condens. Matter. 54 (1996) 3037–3039. doi:10.1103/PhysRevB.54.3037.
[77] H. Sakamoto, H. Tou, H. Ishii, Y. Maniwa, E.A. Reny, S. Yamanaka, NMR studies of superconducting Ba8AgxSi46−x (x=0~6), Phys. C Supercond. 341–348 (2000) 2135–2136. doi:10.1016/S0921-4534(00)01054-6.
[78] Y. Li, R. Zhang, Y. Liu, N. Chen, Z.P. Luo, X. Ma, G. Cao, Z.S. Feng, C.-R. Hu, J.H. Ross, Superconductivity in gallium-substituted Ba 8 Si 46 clathrates, Phys. Rev. B. 75 (2007) 54513. doi:10.1103/PhysRevB.75.054513.
[79] E. Reny, M. Ménétrier, C. Cros, M. Pouchard, J. Sénégas, A 23Na NMR study of NaxSi136 and Na8SI46 silicon clathrates, Comptes Rendus l'Académie Des Sci. - Ser. IIC - Chem. 1 (1998) 129–136. doi:10.1016/S1251-8069(97)86272-0.
[80] J. He, D.D. Klug, K. Uehara, K.F. Preston, C.I. Ratcliffe, J.S. Tse, NMR and X-ray

Spectroscopy of Sodium−Silicon Clathrates, J. Phys. Chem. B. 105 (2001) 3475–3485. doi:10.1021/jp010255e.
[81] R. Castillo, W. Schnelle, M. Bobnar, U. Burkhardt, B. Böhme, M. Baitinger, U. Schwarz, Y. Grin, The Clathrate Ba8-xSi46 Revisited: Preparation Routes, Electrical and Thermal Transport Properties, Zeitschrift Für Anorg. Und Allg. Chemie. 641 (2015) 206–213. doi:10.1002/zaac.201500001.
[82] M. Bobnar, B. Böhme, M. Wedel, U. Burkhardt, A. Ormeci, Y. Prots, C. Drathen, Y. Liang, H.D. Nguyen, M. Baitinger, Y. Grin, Distribution of Al atoms in the clathrate-I phase Ba8AlxSi46−x at x = 6.9, Dalt. Trans. 44 (2015) 12680–12687. doi:10.1039/C5DT01198A.
[83] J. V Zaikina, K.A. Kovnir, U. Burkhardt, W. Schnelle, F. Haarmann, U. Schwarz, Y. Grin, A. V Shevelkov, Cationic Clathrate I Si46-xPxTey (6.6(1) ≤ y ≤ 7.5(1), x ≤ 2y): Crystal Structure, Homogeneity Range, and Physical Properties, Inorg. Chem. 48 (2009) 3720–3730. doi:10.1021/ic8023887.
[84] A. Saramat, G. Svensson, A.E.C. Palmqvist, C. Stiewe, E. Mueller, D. Platzek, S.G.K. Williams, D.M. Rowe, J.D. Bryan, G.D. Stucky, Large thermoelectric figure of merit at high temperature in Czochralski-grown clathrate Ba8Ga16Ge30, J. Appl. Phys. 99 (2006) 23708. doi:10.1063/1.2163979.
[85] D. Arčon, A. Zorko, P. Jeglič, J. Xu, J. Tang, Y. Tanabe, S. Heguri, K. Tanigaki, Rattler Site Selectivity and Covalency Effects in Type-I Clathrates, J. Phys. Soc. Japan. 82 (2013) 14703. doi:10.7566/JPSJ.82.014703.
[86] W. Gou, Y. Li, J. Chi, J.H. Ross, M. Beekman, G.S. Nolas, NMR study of slow atomic motion in Sr8Ga16Ge30 clathrate, Phys. Rev. B. 71 (2005) 174307. doi:10.1103/PhysRevB.71.174307.
[87] R.C. Zamar, C.E. González, Nuclear quadrupole spin-lattice relaxation in anharmonic molecular crystals, Phys. Rev. B. 51 (1995) 932–944. doi:10.1103/PhysRevB.51.932.
[88] H. Tou, K. Sonoda, Y. Nishikawa, H. Kotegawa, H. Suekuni, T. Onimaru, T. Takabatake, NMR Studies of Ba8Ga16Sn30 Clathrates, J. Phys. Soc. Japan. 80 (2011) SA039. doi:10.1143/JPSJS.80SA.SA039.
[89] J.-H. Chen, A. Sirusi Arvij, X. Zheng, S.Y. Rodriguez, J.H. Ross, NMR and computational study of Ba8CuxGe46-x clathrate semiconductors, J. Alloys Compd. 593 (2014) 261–266. doi:10.1016/j.jallcom.2014.01.034.
[90] A.A. Sirusi, J.H. Ross, X. Yan, S. Paschen, NMR study of Ba8Cu5SixGe41−x clathrate semiconductors, Phys. Chem. Chem. Phys. 17 (2015) 16991–16996. doi:10.1039/C5CP02575C.
[91] J. Fulmer, O.I. Lebedev, V. V. Roddatis, D.C. Kaseman, S. Sen, J.A. Dolyniuk, K. Lee, A. V. Olenev, K. Kovnir, Clathrate Ba8Au16P30: The 'gold Standard' for lattice thermal conductivity, J. Am. Chem. Soc. 135 (2013) 12313–12323. doi:10.1021/ja4052679.
[92] J. Gryko, R.F. Marzke, G.A. Lamberton, T.M. Tritt, M. Beekman, G.S. Nolas, Electron structure and temperature-dependent shifts in Cs133 NMR spectra of the Cs8Ge136 clathrate, Phys. Rev. B. 71 (2005) 115208. doi:10.1103/PhysRevB.71.115208.
[93] D. Neiner, N.L. Okamoto, C.L. Condron, Q.M. Ramasse, P. Yu, N.D. Browning, S.M. Kauzlarich, Hydrogen Encapsulation in a Silicon Clathrate Type I Structure: Na5.5(H2)2.15Si46: Synthesis and Characterization, J. Am. Chem. Soc. 129 (2007) 13857–13862. doi:10.1021/ja0724700.
[94] Y. Li, R. Raghavan, N.A. Wagner, S.K. Davidowski, L. Baggetto, R. Zhao, Q. Cheng, J.L.

Yarger, G.M. Veith, C. Ellis-Terrell, M.A. Miller, K.S. Chan, C.K. Chan, Type I Clathrates as Novel Silicon Anodes: An Electrochemical and Structural Investigation, Adv. Sci. 2 (2015) 1500057. doi:10.1002/advs.201500057.
[95] F. Kanetake, A. Harada, H. Mukuda, Y. Kitaoka, T. Rachi, K. Tanigaki, K. M. Itoh, E. E. Haller, 73Ge- and 135/137Ba-NMR Studies of Clathrate Superconductor Ba24Ge100, J. Phys. Soc. Japan. 78 (2009) 104710. doi:10.1143/JPSJ.78.104710.
[96] F. Kanetake, A. Harada, T. Rachi, H. Nagara, H. Mukuda, K. Kusakabe, Y. Kitaoka, N. Suzuki, K. Tanigaki, K. Itoh, E.E. Haller, 73Ge-NMR study and ab initio calculations on clathrate compound Ba24Ge100, J. Phys. Conf. Ser. 121 (2008) 52011. doi:10.1088/1742-6596/121/5/052011.
[97] G.K. Ramachandran, P.F. McMillan, J. Diefenbacher, J. Gryko, J. Dong, O.F. Sankey, 29Si NMR study on the stoichiometry of the silicon clathrate Na8Si46, Phys. Rev. B Condens. Matter Mater. Phys. 60 (1999) 12294–12298. doi:10.1103/PhysRevB.60.12294.
[98] G.K. Ramachandran, J. Dong, O.F. Sankey, P.F. McMillan, 23Na and 29Si NMR Knight shifts in the silicon clathrate Na16Cs8Si136, Phys. Rev. B. 63 (2000) 33102. doi:10.1103/PhysRevB.63.033102.
[99] Y. Maniwa, H. Sakamoto, H. Tou, Y. Aoki, H. Sato, F. Shimizu, H. Kawaji, S. Yamanaka, NMR Studies of Silicon Clathrate Compounds, Mol. Cryst. Liq. Cryst. Sci. Technol. Sect. A. Mol. Cryst. Liq. Cryst. 341 (2000) 497–502. doi:10.1080/10587250008026188.
[100] S. Latturner, B.B. Iversen, J. Sepa, V. Srdanov, G. Stucky, NMR Knight shifts and the electronic properties of Rb8Na16Si136 clathrate, Phys. Rev. B. 63 (2001) 125403. doi:10.1103/PhysRevB.63.125403.
[101] A. Ammar, C. Cros, M. Pouchard, N. Jaussaud, J.-M. Bassat, G. Villeneuve, M. Duttine, M. Ménétrier, E. Reny, On the clathrate form of elemental silicon, Si136: preparation and characterisation of NaxSi136 (x→0), Solid State Sci. 6 (2004) 393–400. doi:10.1016/j.solidstatesciences.2004.02.006.
[102] N. Jaussaud, P. Gravereau, S. Pechev, B. Chevalier, M. Ménétrier, P. Dordor, R. Decourt, G. Goglio, C. Cros, M. Pouchard, n- and p-Type behaviour of the gold-substituted type-I clathrate, Ba8AuxSi46-x (x = 5.4 and 5.9), Comptes Rendus Chim. 8 (2005) 39–46. doi:10.1016/j.crci.2004.12.004.
[103] C.L. Condron, S.M. Kauzlarich, T. Ikeda, G.J. Snyder, F. Haarmann, P. Jeglič, Synthesis, Structure, and High-Temperature Thermoelectric Properties of Boron-Doped Ba8Al14Si31 Clathrate I Phases, Inorg. Chem. 47 (2008) 8204–8212. doi:10.1021/ic800772m.
[104] C.L. Condron, J. Martin, G.S. Nolas, P.M.B. Piccoli, A.J. Schultz, S.M. Kauzlarich, Structure and Thermoelectric Characterization of Ba8Al14Si31, Inorg. Chem. 45 (2006) 9381–9386. doi:10.1021/ic061241w.
[105] S.E. Latturner, J.D. Bryan, N. Blake, H. Metiu, G.D. Stucky, Siting of Antimony Dopants and Gallium in Ba8Ga16Ge30 Clathrates Grown from Gallium Flux, Inorg. Chem. 41 (2002) 3956–3961. doi:10.1021/ic011286r.
[106] C. Uher, Chapter 5 Skutterudites: Prospective novel thermoelectrics, in: Recent Trends Thermoelectr. Mater. Res. I, Academic Press Inc, 2001: pp. 139–253. doi:10.1016/S0080-8784(01)80151-4.
[107] G.S. Nolas, D.T. Morelli, T.M. Tritt, SKUTTERUDITES: A Phonon-Glass-Electron Crystal Approach to Advanced Thermoelectric Energy Conversion Applications, Annu.

Rev. Mater. Sci. 29 (1999) 89–116. doi:10.1146/annurev.matsci.29.1.89.
[108] M. Rull-Bravo, A. Moure, J.F. Fernández, M. Martín-González, Skutterudites as thermoelectric materials: revisited, RSC Adv. 5 (2015) 41653–41667. doi:10.1039/C5RA03942H.
[109] D.T. Morelli, G.P. Meisner, Low temperature properties of the filled skutterudite CeFe4Sb12, J. Appl. Phys. 77 (1995) 3777–3781. doi:10.1063/1.358552.
[110] B.C. Sales, D. Mandrus, R.K. Williams, Filled Skutterudite Antimonides: A New Class of Thermoelectric Materials, Science (80-.). 272 (1996) 1325–1328. doi:10.1126/science.272.5266.1325.
[111] J.P. Fleurial, A. Borshchevsky, T. Caillat, D.T. Morelli, G.P. Meisner, High figure of merit in Ce-filled skutterudites, in: Thermoelectr. 1996., Fifteenth Int. Conf., 1996: pp. 91–95. doi:10.1109/ICT.1996.553263.
[112] X. Shi, J. Yang, J.R. Salvador, M. Chi, J.Y. Cho, H. Wang, S. Bai, J. Yang, W. Zhang, L. Chen, Multiple-Filled Skutterudites: High Thermoelectric Figure of Merit through Separately Optimizing Electrical and Thermal Transports, J. Am. Chem. Soc. 133 (2011) 7837–7846. doi:10.1021/ja111199y.
[113] J.C. Smith, S. Banerjee, V. Pardo, W.E. Pickett, Dirac Point Degenerate with Massive Bands at a Topological Quantum Critical Point, Phys. Rev. Lett. 106 (2011) 56401. doi:10.1103/PhysRevLett.106.056401.
[114] H. Sato, H. Sugawara, Y. Aoki, H. Harima, Magnetic Properties of Filled Skutterudites, Handb. Magn. Mater. 18 (2009) 1–110. doi:10.1016/S1567-2719(09)01801-0.
[115] K. Fujiwara, K. Ishihara, K. Miyoshi, J. Takeuchi, C. Sekine, I. Sirotani, NMR study of spin fluctuations in CeRu4P12, Phys. B Condens. Matter. 281–282 (2000) 296–297. doi:10.1016/S0921-4526(99)01236-3.
[116] K. Magishi, H. Sugawara, T. Saito, K. Koyama, H. Sato, NMR studies of Ce-based filled skutterudites and, Phys. B Condens. Matter. 378–380 (2006) 175–176. doi:10.1016/j.physb.2006.01.067.
[117] K. Fujiwara, NMR study of magnetic properties in SmRu4P12, Phys. B Condens. Matter. 329–333 (2003) 476–477. doi:10.1016/S0921-4526(02)02077-X.
[118] K. Hachitani, H. Amanuma, H. Fukazawa, Y. Kohori, K. Koyama, K. Kumagai, C. Sekine, I. Shirotani, Appearance of Successive Phase Transition in SmRu4P12 under High Magnetic Fields Probed by 31P Nuclear Magnetic Resonance, J. Phys. Soc. Japan. 75 (2006) 124712. doi:10.1143/JPSJ.75.124712.
[119] K. Magishi, Y. Iwahashi, T. Horimoto, H. Sugawara, T. Saito, K. Koyama, NMR study of magnetic properties in filled skutterudite compound, J. Magn. Magn. Mater. 310 (2007) 951–953. doi:10.1016/j.jmmm.2006.10.165.
[120] H. Fukazawa, R. Kobayashi, M. Shimizu, H. Amanuma, K. Hachitani, Y. Komaki, Y. Kohori, K. Akahira, C. Sekine, I. Shirotani, 31P Nuclear Magnetic Resonance and 101Ru Nuclear Quadrupole Resonance Measurements of Filled Skutterudites GdRu4P12 and TbRu4P12, J. Phys. Soc. Japan. 80 (2011) 44713. doi:10.1143/JPSJ.80.044713.
[121] M. Yamamoto, K. Magishi, A. Hisada, T. Saito, K. Koyama, M. Takusari, H. Kato, C. Sekine, NMR Study of Filled Skutterudite Pr0.9Ce0.1Ru4P12, in: Proc. Int. Conf. Strongly Correl. Electron Syst., Journal of the Physical Society of Japan, 2014. doi:10.7566/JPSCP.3.011003.
[122] S. Masaki, T. Mito, S. Wada, H. Sugawara, D. Kikuchi, H. Sato, Dual magnetic correlations in filled skutterudite compound NdRu4P12, Phys. Rev. B. 78 (2008) 94414.

doi:10.1103/PhysRevB.78.094414.
[123] Y. Nakai, K. Ishida, D. Kikuchi, H. Sugawara, H. Sato, Evidence for s-Wave Superconductivity with Antiferromagnetic Fluctuations in Filled Skutterudite LaFe4P12: 139La and 31P-NMR Studies, J. Phys. Soc. Japan. 74 (2005) 3370–3374. doi:10.1143/JPSJ.74.3370.
[124] Y. Tokunaga, T.D. Matsuda, H. Sakai, H. Kato, S. Kambe, R.E. Walstedt, Y. Haga, Y. Ōnuki, H. Yasuoka, 31P-NMR study of the uranium-based filled skutterudite compound UFe4P12, Phys. Rev. B. 71 (2005) 45124. doi:10.1103/PhysRevB.71.045124.
[125] K. Magishi, H. Sugawara, T. Saito, K. Koyama, C. Sekine, K. Takeda, I. Shirotani, NMR Study of Filled Skutterudite with Heavy Lanthanide GdFe4P12 and TbFe4P12, J. Phys. Soc. Japan. 77 (2008) 300–302. doi:10.1143/JPSJS.77SA.300.
[126] O. Sakai, J. Kikuchi, R. Shiina, H. Sato, H. Sugawara, M. Takigawa, H. Shiba, Experimental and theoretical studies of NMR in PrFe4P 12 - Suggestion of antiferro-monopole type ordering, J. Phys. Soc. Japan. 76 (2007) 24710. doi:10.1143/JPSJ.76.024710.
[127] O. Sakai, R. Shiina, H. Shiba, Analysis of hyperfine interactions in NMR studies of Pr skutterudites, J. Phys. Chem. Solids. 68 (2007) 2084–2086. doi:10.1016/j.jpcs.2007.08.031.
[128] J. Kikuchi, M. Takigawa, H. Sugawara, H. Sato, On the Symmetry of Low-Field Ordered Phase of PrFe4P12: 31P NMR, J. Phys. Soc. Japan. 76 (2007) 43705. doi:10.1143/JPSJ.76.043705.
[129] A. Kiss, Y. Kuramoto, Consequence of Spatial Symmetry on 31P NMR Spectra in PrFe4P12 with Scalar Order, J. Phys. Soc. Japan. 77 (2008) 72–77. doi:10.1143/JPSJS.77SA.72.
[130] K. Ishida, H. Murakawa, K. Kitagawa, Y. Ihara, H. Kotegawa, M. Yogi, Y. Kitaoka, B.-L. Young, M.S. Rose, D.E. MacLaughlin, H. Sugawara, T.D. Matsuda, Y. Aoki, H. Sato, H. Harima, Static and dynamical properties in the Pr-based filled skutterudite compound PrFe4P12 revealed by a 31P-NMR study, Phys. Rev. B. 71 (2005) 24424. doi:10.1103/PhysRevB.71.024424.
[131] A. Yamamoto, S. Wada, I. Shirotani, C. Sekine, Low-energy spin fluctuations in heavy-Fermion filled-skutterudite compounds YbFe4P12 and YbFe4Sb12 investigated by 31P-NMR and 121Sb-NQR, J. Magn. Magn. Mater. 310 (2007) 835–837. doi:10.1016/j.jmmm.2006.10.712.
[132] Y. Tokunaga, D. Aoki, Y. Homma, H. Sakai, H. Chudo, S. Kambe, T. D. Matsuda, S. Ikeda, E. Yamamoto, A. Nakamura, Y. Haga, Y. Shiokawa, Y. Ōnuki, H. Yasuoka, 31 P-NMR Study of the Neptunium-based Filled-Skutterudite NpFe4P12, J. Phys. Soc. Japan. 77 (2008) 211–213. doi:10.1143/JPSJS.77SA.211.
[133] Y. Tokunaga, S. Kambe, H. Sakai, H. Chudo, T.D. Matsuda, Y. Haga, H. Yasuoka, D. Aoki, Y. Homma, Y. Shiokawa, Y. Ōnuki, 31P-NMR study of hyperfine interactions and magnetic fluctuations in the neptunium-based filled skutterudite NpFe4P12, Phys. Rev. B. 79 (2009) 54420. doi:10.1103/PhysRevB.79.054420.
[134] K. Magishi, T. Saito, K. Koyama, I. Shirotani, Y. Shimaya, K. Kihou, C. Sekine, N. Takeda, M. Ishikawa, T. Yagi, NMR study of the new filled skutterudite superconductor YFe4P12, Phys. B Condens. Matter. 359–361 (2005) 883–885. doi:10.1016/j.physb.2005.01.333.
[135] K. Magishi, Y. Iwahashi, H. Sugawara, T. Saito, K. Koyama, K. Tanaka, D. Kikuchi, H.

Sato, 31P NMR Study of Filled Skutterudite ROs4P12 (R = La and Pr), J. Phys. Soc. Japan. 77 (2008) 222–224. doi:10.1143/JPSJS.77SA.222.
[136] R. Wawryk, O. Żogał, A. Pietraszko, S. Paluch, T. Cichorek, W.M. Yuhasz, T.A. Sayles, P.-C. Ho, T. Yanagisawa, N.P. Butch, M.B. Maple, Z. Henkie, Crystal structure, 139La NMR and transport properties of the As-based filled skutterudites LaOs4As12 and PrOs4As12, J. Alloys Compd. 451 (2008) 454–456. doi:10.1016/j.jallcom.2007.04.094.
[137] B. Nowak, O. ŻogaŁ, Z. Henkie, M.B. Maple, Multiple quadrupolar spin echoes in the La-filled skutterudite LaOs4As12, Solid State Nucl. Magn. Reson. 36 (2009) 209–211. doi:10.1016/j.ssnmr.2009.12.003.
[138] B. Nowak, O. Zogal, Z. Henkie, M.B. Maple, 139La NMR and 75As NQR study of the As-based filled skutterudite LaOs4As12, Solid State Commun. 151 (2011) 550–552. doi:10.1016/j.ssc.2011.01.012.
[139] B. Nowak, O. Żogał, A. Pietraszko, R.E. Baumbach, M.B. Maple, Z. Henkie, Enhanced spin fluctuations in the As-based filled skutterudite LaFe4As12: A 139L a NMR and 75As NQR study, Phys. Rev. B. 79 (2009) 214411. doi:10.1103/PhysRevB.79.214411.
[140] K. Asaki, H. Kotegawa, H. Tou, S. Tatsuoka, R. Higashinaka, T. Namiki, H. Sato, Anomalous Behavior of Itinerant Weak Ferromagnet LaFe4As12 in NMR/NQR Studies, J. Phys. Soc. Japan. 80 (2011) SA033. doi:10.1143/JPSJS.80SA.SA033.
[141] M. Yogi, H. Niki, T. Kawata, C. Sekine, 75 As-NQR Study of the Kondo Semiconductor CeFe4As12, in: Proc. Int. Conf. Strongly Correl. Electron Syst., Journal of the Physical Society of Japan, 2014: p. 11046. doi:10.7566/JPSCP.3.011046.
[142] M. Toda, H. Sugawara, K. Magishi, T. Saito, K. Koyama, Y. Aoki, H. Sato, Electrical, Magnetic and NMR Studies of Ge-Based Filled Skutterudites RPt4Ge12 (R =La, Ce, Pr, Nd), J. Phys. Soc. Japan. 77 (2008) 124702. doi:10.1143/JPSJ.77.124702.
[143] F. Kanetake, H. Mukuda, Y. Kitaoka, K.I. Magishi, H. Sugawara, K.M. Itoh, E.E. Haller, Superconducting characteristics of filled skutterudites LaPt4Ge12 and PrPt4Ge12: 73Ge-NQR/NMR studies, J. Phys. Soc. Japan. 79 (2010) 63702. doi:10.1143/JPSJ.79.063702.
[144] M. Baenitz, R. Sarkar, R. Gumeniuk, A. Leithe-Jasper, W. Schnelle, H. Rosner, U. Burkhardt, M. Schmidt, U. Schwarz, D. Kaczorowski, Y. Grin, F. Steglich, Ge-based skutterudites MPt4Ge12: A comparative 195Pt NMR study, Phys. Status Solidi. 247 (2010) 740–742. doi:10.1002/pssb.200983043.
[145] V.H. Tran, B. Nowak, A. Jezierski, D. Kaczorowski, Electronic band structure, specific heat, and 195Pt NMR studies of the filled skutterudite superconductor ThPt4Ge12, Phys. Rev. B. 79 (2009) 144510. doi:10.1103/PhysRevB.79.144510.
[146] H. Kotegawa, M. Yogi, Y. Imamura, Y. Kawasaki, G. -q. Zheng, Y. Kitaoka, S. Ohsaki, H. Sugawara, Y. Aoki, H. Sato, Evidence for Unconventional Strong-Coupling Superconductivity in PrOs4Sb12: An Sb Nuclear Quadrupole Resonance Study, Phys. Rev. Lett. 90 (2003) 27001. doi:10.1103/PhysRevLett.90.027001.
[147] M. Yogi, H. Kotegawa, Y. Imamura, G. -q. Zheng, Y. Kitaoka, H. Sugawara, H. Sato, Sb-NQR probe for superconducting properties in the Pr-based filled-skutterudite compound PrRu4Sb12, Phys. Rev. B. 67 (2003) 180501. doi:10.1103/PhysRevB.67.180501.
[148] A. Rabis, A. Leithe-Jasper, A.A. Gippius, E. Morozova, M. Baenitz, W. Schnelle, N. Senthilkumaran, J.A. Mydosh, F. Steglich, Y. Grin, Magnetic resonance investigations on NaFe4Sb12, J. Magn. Magn. Mater. 272–276 (2004) 830–832. doi:10.1016/j.jmmm.2003.11.343.
[149] A. Rabis, M. Baenitz, A. Leithe-Jasper, A.A. Gippius, E.N. Morozova, W. Schnelle, H.

Rosner, J.A. Mydosh, Y. Grin, F. Steglich, 23Na NMR investigations of the itinerant ferromagnets NaFe4Sb12 and Na0.5Ca0.5Fe4Sb12, Phys. B Condens. Matter. 359–361 (2005) 1195–1197. doi:10.1016/j.physb.2005.01.343.
[150] A. Gippius, M. Baenitz, E. Morozova, A. Leithe-Jasper, W. Schnelle, A. Shevelkov, E. Alkaev, A. Rabis, J. Mydosh, Y. Grin, F. Steglich, Crossover between itinerant ferromagnetism and antiferromagnetic fluctuations in filled skutterudites MFe4Sb12 (M=Na, Ba, La) as determined by NMR, J. Magn. Magn. Mater. 300 (2006) e403–e406. doi:10.1016/j.jmmm.2005.10.130.
[151] S. Iemura, A. Yamamoto, S. Wada, I. Shirotani, C. Sekine, Effect of Rare-Earth Filling Rate for the Physical Properties of Skutterudites Investigated through NMR/NQR Measurements, J. Phys. Soc. Japan. 77 (2008) 235–237. doi:10.1143/JPSJS.77SA.235.
[152] M. Yogi, H. Niki, H. Mukuda, Y. Kitaoka, H. Sugawara, H. Sato, Sb-NMR study of filled skutterudite CeOs4Sb12, J. Magn. Magn. Mater. 310 (2007) 941–943. doi:10.1016/j.jmmm.2006.10.155.
[153] M. Matsumura, H. Kato, T. Nishioka, E. Matsuoka, K. Hayashi, T. Takabatake, Nearly ferromagnetic state probed by Sb-NQR in filled skutterudite La0.88Fe4Sb12, J. Magn. Magn. Mater. 310 (2007) 1035–1037. doi:10.1016/j.jmmm.2006.10.228.
[154] C.S. Lue, S.M. Huang, C.N. Kuo, F.-T. Huang, M.-W. Chu, Effect of partial La filling on the local electronic properties of LaxCo4Sb12 studied using 59Co NMR, New J. Phys. 10 (2008) 83029. doi:10.1088/1367-2630/10/8/083029.
[155] C.S. Lue, S.C. Chen, Evolution of the electronic structure in partially filled skutterudites: CaxCo4Sb12 studied using NMR, Phys. Rev. B. 79 (2009) 125108. doi:10.1103/PhysRevB.79.125108.
[156] M. Matsumura, G. Hyoudou, M. Itoh, H. Kato, T. Nishioka, E. Matsuoka, H. Tou, T. Takabatake, M. Sera, Unusual suppression of low energy spin excitations near Fermi level in AFe4Sb12 (A = Ca, Sr, and Ba) probed by Sb-NQR, J. Phys. Soc. Japan. 76 (2007) 84716. doi:10.1143/JPSJ.76.084716.
[157] K.-I. Magishi, H. Sugawara, I. Mori, T. Saito, K. Koyama, Sb-NQR study of filled skutterudite CeFe4Sb12, J. Phys. Chem. Solids. 68 (2007) 2076–2079. doi:10.1016/j.jpcs.2007.08.030.
[158] Y. Nakai, K. Ishida, K. Magishi, H. Sugawara, D. Kikuchi, H. Sato, Rattling phonons in the filled skutterudite LaT4X12(T=Fe,Ru,Os;X=P,Sb) studied with La-NMR, P-NMR/Sb-NQR, J. Magn. Magn. Mater. 310 (2007) 255–257. doi:10.1016/j.jmmm.2006.10.035.
[159] A. Yamamoto, S. Iemura, S. Wada, K. Ishida, I. Shirotani, C. Sekine, Low-energy spin fluctuations in filled skutterudites YbFe4Sb12 and LaFe4Sb12 investigated through 121Sb nuclear quadrupole and 139La nuclear magnetic resonance measurements, J. Phys. Condens. Matter. 20 (2008) 195214. doi:10.1088/0953-8984/20/19/195214.
[160] M. Yogi, H. Niki, M. Yashima, H. Mukuda, Y. Kitaoka, H. Sugawara, H. Sato, Magnetic Field Evolution of a Novel Phase Transition in CeOs4Sb12: 121Sb NMR Study, J. Phys. Soc. Japan. 78 (2009) 53703. doi:10.1143/JPSJ.78.053703.
[161] H. Tou, Y. Inaoka, M. Doi, M. Sera, K. Asaki, H. Kotegawa, H. Sugawara, H. Sato, Possible Mass Enhancement by Multipole Fluctuations Excited via the Singlet–Triplet Crystal Electric Field States in PrOs4Sb12 : Sb-NMR Studies Using a Single Crystal, J. Phys. Soc. Japan. 80 (2011) 74703. doi:10.1143/JPSJ.80.074703.
[162] M. Yogi, H. Niki, H. Sugawara, N. Takeda, H. Sato, Electric Field Gradient Fluctuations in Filled Skutterudite ReRu4Sb12 (Re = La, Ce, and Pr) Probed by Sb-NQR, J. Phys. Soc.

Japan. 80 (2011) SA027. doi:10.1143/JPSJS.80SA.SA027.
[163] M. Yogi, H. Niki, H. Mukuda, Y. Kitaoka, H. Sugawara, H. Sato, 121 Sb-NMR Knight shift study of filled skutterudite CeOs4Sb12, J. Phys. Conf. Ser. 391 (2012) 12080. doi:10.1088/1742-6596/391/1/012080.
[164] K. Magishi, H. Sugawara, M. Takahashi, T. Saito, K. Koyama, T. Saito, S. Tatsuoka, K. Tanaka, H. Sato, Effects of Filling Fraction on Magnetic Properties of Filled Skutterudite RFe4Sb12 (R = La, Ce) Synthesized under High Pressure, J. Phys. Soc. Japan. 81 (2012) 124706. doi:10.1143/JPSJ.81.124706.
[165] K. Magishi, M. Takahashi, T. Saito, K. Koyama, H. Sugawara, T. Saito, S. Tatsuoka, K. Tanaka, H. Sato, Sb NQR study of the filled skutterudite CeFe4Sb12 synthesized under high pressure, J. Korean Phys. Soc. 63 (2013) 804–808. doi:10.3938/jkps.63.804.
[166] K. Magishi, Y. Nakai, K. Ishida, H. Sugawara, I. Mori, T. Saito, K. Koyama, Evidence for ferromagnetic fluctuations in filled skutterudite LaFe4Sb12 : Sb-NQR and La-NMR, J. Phys. Soc. JAPAN. 75 (2006). doi:10.1143/JPSJ.75.023701.
[167] K.M. Agishi, T.K. Usaka, A.H. Isada, T.S. Aito, K. Oyama, H.S. Ugawara, Y.S. Ekihara, H.A. Oki, NMR/NQR Study of Filled Skutterudite La0.5Co4Sb12, Proc. Int. Conf. Strongly Correl. Electron Syst. 3 (2014) 11064. doi:10.7566/JPSCP.3.011064.
[168] D.J. Singh, W.E. Pickett, Skutterudite antimonides: Quasilinear bands and unusual transport, Phys. Rev. B. 50 (1994) 11235–11238. doi:10.1103/PhysRevB.50.11235.
[169] W. Li, N. Mingo, Thermal conductivity of fully filled skutterudites: Role of the filler, Phys. Rev. B. 89 (2014) 184304. doi:10.1103/PhysRevB.89.184304.
[170] R. Hanus, X. Guo, Y. Tang, G. Li, G.J. Snyder, W.G. Zeier, A Chemical Understanding of the Band Convergence in Thermoelectric CoSb3 Skutterudites: Influence of Electron Population, Local Thermal Expansion, and Bonding Interactions, Chem. Mater. 29 (2017) 1156–1164. doi:10.1021/acs.chemmater.6b04506.
[171] J.B. Boyce, B.A. Huberman, Superionic conductors: Transitions, structures, dynamics, Phys. Rep. 51 (1979) 189–265. doi:10.1016/0370-1573(79)90067-X.
[172] S. Ishiwata, Y. Shiomi, J.S. Lee, M.S. Bahramy, T. Suzuki, M. Uchida, R. Arita, Y. Taguchi, Y. Tokura, Extremely high electron mobility in a phonon-glass semimetal, Nat. Mater. 12 (2013) 512–517. doi:10.1038/nmat3621.
[173] W. Zhang, R. Yu, W. Feng, Y. Yao, H. Weng, X. Dai, Z. Fang, Topological Aspect and Quantum Magnetoresistance of β-Ag2Te, Phys. Rev. Lett. 106 (2011) 156808. doi:10.1103/PhysRevLett.106.156808.
[174] S. Rehman, K. Kim, J.-H. Hur, D. Kim, Phase transformation induced resistive switching behavior in Al/Cu2Se/Pt, J. Phys. D. Appl. Phys. 50 (2017) 135301. doi:10.1088/1361-6463/aa593e.
[175] S.D. Kang, S.A. Danilkin, U. Aydemir, M. Avdeev, A. Studer, G.J. Snyder, Apparent critical phenomena in the superionic phase transition of Cu2-xSe, New J. Phys. 18 (2016) 13024. doi:10.1088/1367-2630/18/1/013024.
[176] S. Ballikaya, H. Chi, J.R. Salvador, C. Uher, Thermoelectric properties of Ag-doped Cu2Se and Cu2Te, J. Mater. Chem. A. 1 (2013). doi:10.1039/c3ta12508d.
[177] C. Shi, X. Xi, Z. Hou, E. Liu, W. Wang, S. Jin, Y. Wu, G. Wu, Atomic-Level Characterization of Dynamics of Copper Ions in CuAgSe, J. Phys. Chem. C. 120 (2016) 3229–3234. doi:10.1021/acs.jpcc.5b12296.
[178] C. Shi, X. Xi, Z. Hou, E. Liu, W. Wang, J. Chen, G. Wu, Copper dynamics and structural-transformation in noble metal chalcogenides CuAgS probed by 63Cu NMR, Solid State

Ionics. 300 (2017) 182–186. doi:10.1016/j.ssi.2016.12.029.
[179] S. Hébert, A. Maignan, Thermoelectric Oxides, in: Funct. Oxides, John Wiley & Sons, Ltd, Chichester, UK, 2010: pp. 203–255. doi:10.1002/9780470686072.ch4.
[180] I. Terasaki, Y. Sasago, K. Uchinokura, Large thermoelectric power in NaCo2O4 single crystals, Phys. Rev. B. 56 (1997) R12685–R12687. doi:10.1103/PhysRevB.56.R12685.
[181] Y. Wang, N.S. Rogado, R.J. Cava, N.P. Ong, Spin entropy as the likely source of enhanced thermopower in NaxCo2O4, Nature. 423 (2003) 425–428. doi:10.1038/nature01639.
[182] K. Koumoto, I. Terasaki, R. Funahashi, Complex Oxide Materials for Potential Thermoelectric Applications, MRS Bull. 31 (2006) 206–210. doi:10.1557/mrs2006.46.
[183] J. Bobroff, G. Lang, H. Alloul, N. Blanchard, G. Collin, NMR Study of the Magnetic and Metal-Insulator Transitions in Na0.5CoO2 : A Nesting Scenario, Phys. Rev. Lett. 96 (2006) 107201. doi:10.1103/PhysRevLett.96.107201.
[184] B. Pedrini, J.L. Gavilano, S. Weyeneth, E. Felder, J. Hinderer, M. Weller, H.R. Ott, S.M. Kazakov, J. Karpinski, Magnetic phase transition at 88K in Na0.5CoO2 revealed by 23Na NMR investigations, Phys. Rev. B. 72 (2005) 214407. doi:10.1103/PhysRevB.72.214407.
[185] M. Itoh, M. Nagawatari, NMR study of two-dimensional cobalt oxide with large thermoelectric power NaCo2O4, Phys. B Condens. Matter. 281–282 (2000) 516–517. doi:10.1016/S0921-4526(99)01042-X.
[186] F.L. Ning, S.M. Golin, K. Ahilan, T. Imai, G.J. Shu, F.C. Chou, 59Co NMR Evidence for Charge Ordering below TCO~51 K in Na0.5CoO2, Phys. Rev. Lett. 100 (2008) 86405. doi:10.1103/PhysRevLett.100.086405.
[187] M. Yokoi, Y. Kobayashi, T. Moyoshi, M. Sato, NMR Studies of Successive Phase Transitions in Na0.5CoO2 and K0.5CoO 2, J. Phys. Soc. Japan. 77 (2008) 74704. doi:10.1143/JPSJ.77.074704.
[188] M. Yokoi, T. Moyoshi, Y. Kobayashi, M. Soda, Y. Yasui, M. Sato, K. Kakurai, Magnetic Correlation of NaxCoO2 and Successive Phase Transitions of Na0.5CoO2 –NMR and Neutron Diffraction Studies–, J. Phys. Soc. Japan. 74 (2005) 3046–3056. doi:10.1143/JPSJ.74.3046.
[189] Y. Kobayashi, M. Yokoi, T. Moyoshi, H. Watanabe, M. Sato, NMR studies of successive transition in Na0.5CoO2, J. Magn. Magn. Mater. 310 (2007) 675–677. doi:10.1016/j.jmmm.2006.10.175.
[190] H. Watanabe, Y. Mori, M. Yokoi, T. Moyoshi, M. Soda, Y. Yasui, Y. Kobayashi, M. Sato, N. Igawa, K. Kakurai, Magnetic and Metal–Insulator Transitions in β-Na0.5CoO2 and γ-K0.5CoO2 –NMR and Neutron Diffraction Studies–, J. Phys. Soc. Japan. 75 (2006) 34716. doi:10.1143/JPSJ.75.034716.
[191] R. Ray, A. Ghoshray, K. Ghoshray, S. Nakamura, 59Co NMR studies of metallic NaCo2O4, Phys. Rev. B. 59 (1999) 9454–9461. doi:10.1103/PhysRevB.59.9454.
[192] J.L. Gavilano, B. Pedrini, K. Magishi, J. Hinderer, M. Weller, H.R. Ott, S.M. Kazakov, J. Karpinski, Localized versus itinerant magnetic moments in Na0.7CoO2, Phys. Rev. B. 74 (2006) 64410. doi:10.1103/PhysRevB.74.064410.
[193] T.A. Platova, I.R. Mukhamedshin, H. Alloul, A. V. Dooglav, G. Collin, Nuclear quadrupole resonance and x-ray investigation of the structure of Na2/3CoO2, Phys. Rev. B. 80 (2009) 224106. doi:10.1103/PhysRevB.80.224106.
[194] I.R. Mukhamedshin, H. Alloul, 59Co NMR evidence for charge and orbital order in the kagome-like structure of Na2/3CoO2, Phys. Rev. B. 84 (2011) 155112.

doi:10.1103/PhysRevB.84.155112.
[195] H. Alloul, I.R. Mukhamedshin, T.A. Platova, A. V. Dooglav, Na ordering imprints a metallic kagomé lattice onto the Co planes of Na2/3CoO2, EPL (Europhysics Lett. 85 (2009) 47006. doi:10.1209/0295-5075/85/47006.
[196] H. Alloul, I.R. Mukhamedshin, A. V. Dooglav, Y. V. Dmitriev, V.-C. Ciomaga, L. Pinsard-Gaudart, G. Collin, 23Na NMR study of sodium order in NaxCoO2 with 22 K Néel temperature, Phys. Rev. B. 85 (2012) 134433. doi:10.1103/PhysRevB.85.134433.
[197] B.-L. Young, P.-Y. Chu, J.Y. Juang, G.J. Shu, F.C. Chou, Cobalt magnetism in a superstructured metallic antiferromagnet Na0.825CoO2, Phys. Rev. B. 88 (2013) 64418. doi:10.1103/PhysRevB.88.064418.
[198] J. Bobroff, S. Hébert, G. Lang, P. Mendels, D. Pelloquin, A. Maignan, Interplay between magnetic properties and thermoelectricity in misfit and Na cobaltates, Phys. Rev. B. 76 (2007) 100407(R). doi:10.1103/PhysRevB.76.100407.
[199] E. V. Sampathkumaran, N. Fujiwara, S. Rayaprol, P.K. Madhu, Y. Uwatoko, Magnetic behavior of Co ions in the exotic spin-chain compound Ca3Co2O6 from 59Co NMR studies, Phys. Rev. B. 70 (2004) 14437. doi:10.1103/PhysRevB.70.014437.
[200] Y. Shimizu, M. Horibe, H. Nanba, T. Takami, M. Itoh, Anisotropic spin dynamics in the frustrated chain Ca3Co2O6 detected by single-crystal 59Co NMR, Phys. Rev. B. 82 (2010) 94430. doi:10.1103/PhysRevB.82.094430.
[201] G. Allodi, R. De Renzi, S. Agrestini, C. Mazzoli, M.R. Lees, NMR study of magnetic order, metamagnetic transitions, and low-temperature spin freezing in Ca3Co2O6, Phys. Rev. B. 83 (2011) 104408. doi:10.1103/PhysRevB.83.104408.
[202] G. Allodi, P. Santini, S. Carretta, S. Agrestini, C. Mazzoli, A. Bombardi, M.R. Lees, R. De Renzi, Exchange interactions in Ca3Co2O6 probed locally by NMR, Phys. Rev. B. 89 (2014) 104401. doi:10.1103/PhysRevB.89.104401.
[203] T. Takami, H. Nanba, Y. Umeshima, M. Itoh, H. Nozaki, H. Itahara, J. Sugiyama, Phase separation in the CoO2 layer observed in thermoelectric layered cobalt dioxides, Phys. Rev. B. 81 (2010) 14401. doi:10.1103/PhysRevB.81.014401.
[204] T. Takami, Y. Umeshima, H. Nanba, M. Itoh, 59Co NMR study on local magnetic properties of misfit layered Co oxides with rocksalt-type and CoO2 layers, J. Phys. Conf. Ser. 150 (2009) 42199. doi:10.1088/1742-6596/150/4/042199.
[205] S. Fan, J. Zhao, J. Guo, Q. Yan, J. Ma, H.H. Hng, p-type Bi0.4Sb1.6Te3 nanocomposites with enhanced figure of merit, Appl. Phys. Lett. 96 (2010) 182104. doi:10.1063/1.3427427.
[206] K.F. Hsu, Cubic AgPbmSbTe2+m: Bulk Thermoelectric Materials with High Figure of Merit, Science (80-.). 303 (2004) 818–821. doi:10.1126/science.1092963.
[207] E.M. Levin, S.L. Bud'ko, K. Schmidt-Rohr, Enhancement of Thermopower of TAGS-85 High-Performance Thermoelectric Material by Doping with the Rare Earth Dy, Adv. Funct. Mater. 22 (2012) 2766–2774. doi:10.1002/adfm.201103049.
[208] J. Cui, E.M. Levin, Y. Lee, Y. Furukawa, Electronic properties of GeTe and Ag- or Sb-substituted GeTe studied by low-temperature 125Te NMR, Phys. Rev. B. 94 (2016) 85203. doi:10.1103/PhysRevB.94.085203.
[209] S.N. Girard, K. Schmidt-Rohr, T.C. Chasapis, E. Hatzikraniotis, B. Njegic, E.M. Levin, A. Rawal, K.M. Paraskevopoulos, M.G. Kanatzidis, Analysis of Phase Separation in High Performance PbTe-PbS Thermoelectric Materials, Adv. Funct. Mater. 23 (2013) 747–757. doi:10.1002/adfm.201201944.

[210] E.M. Levin, B.A. Cook, K. Ahn, M.G. Kanatzidis, K. Schmidt-Rohr, Electronic inhomogeneity and Ag:Sb imbalance of Ag1−yPb18Sb1+zTe20 high-performance thermoelectrics elucidated by 125Te and 207Pb NMR, Phys. Rev. B. 80 (2009) 115211. doi:10.1103/PhysRevB.80.115211.
[211] S. Boutin, J. Ramírez-Ruiz, I. Garate, Tight-binding theory of NMR shifts in topological insulators Bi2Se3 and Bi2Te3, Phys. Rev. B. 94 (2016) 115204. doi:10.1103/PhysRevB.94.115204.
[212] D. Koumoulis, T.C. Chasapis, R.E. Taylor, M.P. Lake, D. King, N.N. Jarenwattananon, G.A. Fiete, M.G. Kanatzidis, L.-S. Bouchard, NMR Probe of Metallic States in Nanoscale Topological Insulators, Phys. Rev. Lett. 110 (2013) 26602. doi:10.1103/PhysRevLett.110.026602.
[213] D.Y. Podorozhkin, E. V. Charnaya, A. Antonenko, R. Mukhamad'yarov, V. V. Marchenkov, S. V. Naumov, J.C.A. Huang, H.W. Weber, A.S. Bugaev, Nuclear magnetic resonance study of a Bi2Te3 topological insulator, Phys. Solid State. 57 (2015) 1741–1745. doi:10.1134/S1063783415090279.
[214] E.M. Levin, T.M. Riedemann, A. Howard, N.H. Jo, S.L. Bud'ko, P.C. Canfield, T.A. Lograsso, 125Te NMR and Seebeck Effect in Bi2Te 3 Synthesized from Stoichiometric and Te-Rich Melts, J. Phys. Chem. C. 120 (2016) 25196–25202. doi:10.1021/acs.jpcc.6b06973.
[215] D. Koumoulis, R.E. Taylor, D. King, L.-S. Bouchard, NMR study of native defects in PbSe, Phys. Rev. B. 90 (2014) 125201. doi:10.1103/PhysRevB.90.125201.
[216] T.C. Chasapis, D. Koumoulis, B. Leung, N.P. Calta, S.-H. Lo, V.P. Dravid, L.-S. Bouchard, M.G. Kanatzidis, Two-band model interpretation of the p- to n- transition in ternary tetradymite topological insulators, APL Mater. 3 (2015) 83601. doi:10.1063/1.4922857.
[217] D. Koumoulis, T.C. Chasapis, B. Leung, R.E. Taylor, C.C. Stoumpos, N.P. Calta, M.G. Kanatzidis, L.-S. Bouchard, Site-Specific Contributions to the Band Inversion in a Topological Crystalline Insulator, Adv. Electron. Mater. 1 (2015) 1500117. doi:10.1002/aelm.201500117.
[218] T.G. Edwards, E.L. Gjersing, S. Sen, S.C. Currie, B.G. Aitken, 125Te NMR chemical shifts and tellurium coordination environments in crystals and glasses in the Ge–As–Sb–Te system, J. Non. Cryst. Solids. 357 (2011) 3036–3041. doi:10.1016/j.jnoncrysol.2011.04.007.
[219] E.M. Levin, M.F. Besser, R. Hanus, Electronic and thermal transport in GeTe: A versatile base for thermoelectric materials, J. Appl. Phys. 114 (2013) 83713. doi:10.1063/1.4819222.
[220] E.M. Levin, R. Hanus, M. Hanson, W.E. Straszheim, K. Schmidt-Rohr, Thermoelectric properties of Ag2Sb2Ge46−xDyxTe50 alloys with high power factor, Phys. Status Solidi. 210 (2013) 2628–2637. doi:10.1002/pssa.201330217.
[221] E.M. Levin, M.J. Kramer, K. Schmidt-Rohr, Local composition and carrier concentration in Pb0.7Ge0.3Te and Pb0.5Ge0.5Te alloys from 125Te NMR and microscopy, J. Phys. Chem. Solids. 75 (2014) 1269–1276. doi:10.1016/j.jpcs.2014.06.004.
[222] E.M. Levin, J.-F. Cui, K. Schmidt-Rohr, Sub-millisecond 125Te NMR spin-lattice relaxation times and large Knight shifts in complex tellurides: Validation of a quadratic relation across the spectrum, Solid State Nucl. Magn. Reson. 78 (2016) 40–44. doi:10.1016/j.ssnmr.2016.07.003.

[223] E.M. Levin, Effects of Ge substitution in GeTe by Ag or Sb on the Seebeck coefficient and carrier concentration derived from 125Te NMR, Phys. Rev. B. 93 (2016) 45209. doi:10.1103/PhysRevB.93.045209.
[224] S. Chen, Z. Ren, Recent progress of half-Heusler for moderate temperature thermoelectric applications, Mater. Today. 16 (2013) 387–395. doi:10.1016/j.mattod.2013.09.015.
[225] J. Carrete, W. Li, N. Mingo, S. Wang, S. Curtarolo, Finding Unprecedentedly Low-Thermal-Conductivity Half-Heusler Semiconductors via High-Throughput Materials Modeling, Phys. Rev. X. 4 (2014) 11019. doi:10.1103/PhysRevX.4.011019.
[226] G.J. Poon, Chapter 2 Electronic and thermoelectric properties of Half-Heusler alloys, in: 2001: pp. 37–75. doi:10.1016/S0080-8784(01)80136-8.
[227] T. Zhu, C. Fu, H. Xie, Y. Liu, X. Zhao, High Efficiency Half-Heusler Thermoelectric Materials for Energy Harvesting, Adv. Energy Mater. 5 (2015) 1500588. doi:10.1002/aenm.201500588.
[228] B. Nowak, D. Kaczorowski, NMR as a Probe of Band Inversion in Topologically Nontrivial Half-Heusler Compounds, J. Phys. Chem. C. 118 (2014) 18021–18026. doi:10.1021/jp505320w.
[229] C. Shi, X. Xi, Z. Hou, X. Zhang, G. Xu, E. Liu, W. Wang, W. Wang, J. Chen, G. Wu, NMR investigation of atomic and electronic structures of half-Heusler topologically nontrivial semimetals, Phys. Status Solidi. 252 (2015) 357–360. doi:10.1002/pssb.201451436.
[230] X. Zhang, Z. Hou, Y. Wang, G. Xu, C. Shi, E. Liu, X. Xi, W. Wang, G. Wu, X. Zhang, NMR Evidence for the Topologically Nontrivial Nature in a Family of Half-Heusler Compounds, Sci. Rep. 6 (2016) 23172. doi:10.1038/srep23172.
[231] C.S. Lue, Y. Oner, D.G. Naugle, J.H. Ross, Magnetism of new semi-Heusler compounds FeVSn and CoVSn, IEEE Trans. Magn. 37 (2001) 2138–2140. doi:10.1109/20.951101.
[232] a. Grykałowska, K. Wochowski, B. Nowak, Semi-Heusler-type intermetallics MPtSn (M=Ti, Zr, Hf, Th): a magnetic susceptibility and NMR study, Intermetallics. 13 (2005) 756–763. doi:10.1016/j.intermet.2004.11.003.
[233] a Grykałowska, B. Nowak, High-resolution solid-state 119Sn and 195Pt NMR studies of MPtSn semiconductors (M = Ti, Zr, Hf, Th)., Solid State Nucl. Magn. Reson. 27 (2005) 223–7. doi:10.1016/j.ssnmr.2004.11.006.
[234] H. Nishihara, T. Kanomata, Y. Furutani, T. Igarashi, K. Koyama, T. Goto, NMR properties of half-Heusler CoVSb, Phys. Status Solidi. 3 (2006) 2779–2782. doi:10.1002/pssc.200669642.
[235] A. Grykałowska, M. Wołcyrz, B. Nowak, Orbital ordering in the half-Heusler-type compound UPtSn: Evidence from 119Sn and 195Pt NMR studies, Phys. Rev. B. 73 (2006) 212404. doi:10.1103/PhysRevB.73.212404.
[236] V. Ksenofontov, G. Melnyk, M. Wojcik, S. Wurmehl, K. Kroth, S. Reiman, P. Blaha, C. Felser, Structure and properties of CoMnSb in the context of half-metallic ferromagnetism, Phys. Rev. B. 74 (2006) 134426. doi:10.1103/PhysRevB.74.134426.
[237] a. Grykałowska, B. Nowak, Half-Heusler compounds UPtSn and ThPtSn: and NMR studies, J. Alloys Compd. 453 (2008) 7–14. doi:10.1016/j.jallcom.2006.11.072.
[238] T. Harmening, H. Eckert, R. Pöttgen, Defects in half-Heusler type antimonides ScTSb (T=Ni, Pd, Pt), Solid State Sci. 11 (2009) 900–906. doi:10.1016/j.solidstatesciences.2008.12.007.
[239] T. Koyama, M. Abe, T. Mito, K. Ueda, T. Kohara, H. S. Suzuki, NMR Studies of Half-

Heusler Type Compounds YbPtSb and LuPtSb, J. Phys. Soc. Japan. 80 (2011) SA097. doi:10.1143/JPSJS.80SA.SA097.
[240] B. Nowak, D. Kaczorowski, Nonmetallic behaviour in half-Heusler phases YPdSb, YPtSb and LuPtSb, Intermetallics. 40 (2013) 28–35. doi:10.1016/j.intermet.2013.04.001.
[241] S. Dupke, H. Eckert, F. Winter, R. Pöttgen, A systematic solid state NMR spectroscopic study of the equiatomic lithium half-Heusler phases LiTX (T = Mg, Zn, Cd; X = P, As, Sb, Bi), Prog. Solid State Chem. 42 (2014) 57–64. doi:10.1016/j.progsolidstchem.2014.04.002.
[242] B. Nowak, O. Pavlosiuk, D. Kaczorowski, Band Inversion in Topologically Nontrivial Half-Heusler Bismuthides: 209 Bi NMR Study, J. Phys. Chem. C. (2015) 150123144728006. doi:10.1021/jp5115493.
[243] C. Benndorf, H. Eckert, R. Pöttgen, 29Si, 47Ti, 49Ti and 195Pt solid state MAS NMR spectroscopic investigations of ternary silicides TPtSi, germanides TPtGe (T = Ti, Zr, Hf) and stannide TiPtSn, Dalt. Trans. 45 (2016) 8215–8223. doi:10.1039/C6DT00861E.
[244] B. Nowak, D. Kaczorowski, 209Bi NMR in Topologically Trivial and Nontrivial Half-Heusler Bismuthides, J. Phys. Chem. C. 120 (2016) 21797–21801. doi:10.1021/acs.jpcc.6b07135.